J. Fluid Mech. (1989), *vol.* 208, *pp.* 161–192
Printed in Great Britain

Buoyancy-driven motion of a deformable drop through a quiescent liquid at intermediate Reynolds numbers

By DAVID S. DANDY[1] AND L. GARY LEAL[2]

[1] Combustion Research Facility, Sandia National Laboratories, Livermore, CA 94551, USA
[2] Department of Chemical Engineering, Caltech, Pasadena, CA 91125, USA

(Received 24 October 1988)

Numerical solutions have been obtained for steady streaming flow past an axisymmetric drop over a wide range of Reynolds numbers ($0.005 \leqslant Re \leqslant 250$), Weber numbers ($0.005 \leqslant We \leqslant 14$), viscosity ratios ($0.001 \leqslant \lambda \leqslant 1000$), and density ratios ($0.001 \leqslant \zeta \leqslant 1000$). Our results indicate that at lower Reynolds numbers the shape of the drop tends toward a spherical cap with increasing We, but at higher Re the body becomes more disk shaped with increasing We. Unlike the recirculating wake behind an inviscid bubble or solid particle, the eddy behind a drop is detached from the interface. The size of the eddy and the separation distance from the drop depend on the four dimensionless parameters of the problem. The motion of the fluid inside the drop appears to control the behaviour of the external flow near the body, and even for cases when λ and $\zeta \ll 1$ (a 'real' bubble), a recirculating wake remains unattached.

1. Introduction

The buoyancy-driven motion of drops and bubbles plays a critical role in many areas of the chemical engineering industry. Such diverse processes as liquid–liquid extraction, flotation, sedimentation, and combustion all rely on the dispersion of one fluid phase in another. As a consequence, a great deal of experimental work has been done to study the buoyancy-driven motion of bubbles, drops, and particles (Clift, Grace & Weber (1978) provide a thorough survey of both theoretical and experimental work), and approximate theoretical solutions have been obtained for drops and bubbles in the limit of very small deformation for either high (Moore 1959, 1963, 1965; Harper & Moore 1968; Parlange 1970; Harper 1972) or low (Taylor & Acrivos 1964; Brignell 1973) Reynolds number. Until recently, however, the motion of drops and bubbles with a finite degree of deformation could not be studied theoretically owing to the lack of effective methods for dealing with the unknown shape of the free-surface. The first successful resolution of this difficulty was reported by Ryskin & Leal (1984*a*, *b*) and Christov & Volkov (1985), both of whom obtained numerical solutions for the steady rise of a deformable inviscid bubble, without an intrinsic limitation on the degree of bubble deformation. Ryskin & Leal's solutions encompass Reynolds and Weber numbers in the ranges $1 \leqslant We \leqslant 20$ and $1 \leqslant Re \leqslant 200$, and show a dramatic variety of shapes and flows. The present paper presents a numerical study of the corresponding solutions for steady, axisymmetric motion of a viscous drop.

One motivation for this work is to show that the numerical scheme of Ryskin &

Leal (1983) can be modified successfully to solve free-boundary problems which involve two fluids (rather than one viscous fluid and a void with $\rho = \mu = 0$ as in the original applications, Ryskin & Leal 1984*a*, *b*). From the viewpoint of fluid mechanics, the goals of the present work are broadly to study the solution behaviour – flow field and drop shape – as a function of the four dimensionless parameters of the problem: the Reynolds number Re, Weber number We, viscosity ratio λ, and density ratio ζ. Practical interest in the results is primarily for prediction of the terminal velocity (or, equivalently, the hydrodynamic drag) as a function of the four independent dimensionless parameters and, also, as a precursor to numerical predictions of transport rates in mass transfer applications. However, there are a number of fundamental, fluid mechanics issues which also motivate the present study. Foremost among these is the structure of the wake behind the drop, and the associated problems of vorticity transport and production at an interface at finite Reynolds number. The drop is of special interest, in this regard. First, existing experimental studies (Garner & Tayeban 1960, and LeClair 1970) indicate that a recirculating wake appears (as is also true for bubbles and solid particles), but that the eddy is detached from the drop surface. We have suggested previously, based upon numerical investigation of the wake structure behind a bubble, that recirculating wakes at Reynolds numbers of $O(10^2)$ should be viewed as being a consequence of vorticity accumulation rather than a finite-Reynolds-number version of the separation process that is described by boundary-layer theory for the asymptotic limit $Re \to \infty$. Clearly, a detached recirculating wake cannot be explained as a manifestation of the latter type of separation – there is not even a detachment or separation point at the drop surface. We suggest that the relevant mechanism must again be vorticity accumulation, but it is extremely interesting to try to understand why this leads to a detached wake for a drop, when almost all other known examples of recirculating wakes are attached. (However, see Leal & Acrivos 1969 for another example of a detached recirculating wake at finite Reynolds number.) A second intriguing feature of the viscous drop, from a fundamental point of view is that vorticity is produced by a combination of a 'no-slip' mechanism that is typical of a solid body and by the surface mechanism that is typical of the free-shear surface for a bubble or void. The relative importance of these two mechanisms for a drop is controlled primarily by the viscosity ratio λ. Of particular interest is the relationship between the rate of vorticity production for large Reynolds numbers and the wake structure, compare with Dandy & Leal (1986). For a no-slip surface, $\omega_s \sim Re^{\frac{1}{2}}$ while, for a slip surface of fixed curvature, $\omega_s \sim O(1)$ for $Re \gg 1$. The viscous drop allows some insight into the transition between these two extremes. Finally, there are a number of unresolved questions about the stability of shape and rise trajectory for both bubbles and drops. The solutions reported here, as well as those of Ryskin & Leal (1984*a*, *b*), provide a starting point for understanding and analysing these instabilities.

To facilitate the study of this problem, we employ the boundary-fitted orthogonal curvilinear coordinate grid generation technique of Ryskin & Leal (1983). It is not necessary to describe the method here except to note that since it is boundary-fitted, the free surface of the droplet corresponds to a coordinate line in the computational domain, thereby avoiding the problems associated with interpolation between node points to provide approximate boundary conditions. Further, there are two routes that are available when using this grid generation technique. The first is called the strong constraint method and is very useful for free-boundary problems. The second is referred to as the weak constraint method, and is useful when it is necessary to

specify the positions of nodal points on the boundary. In this work we have used the strong constraint method to generate the outer coordinate grid and the weak constraint method to generate the grid inside the drop. The reasons for this will be discussed shortly.

2. Problem statement

In this section we shall discuss the formulation of the problem and the method of solution. We consider a viscous droplet that is assumed to undergo a steady rectilinear motion, due to the action of gravity, through an outer quiescent liquid. The drop phase is characterized by a constant viscosity $\hat{\mu}$ and density $\hat{\rho}$. (Quantities associated with the drop fluid will be denoted by $\hat{}$.) Likewise, the outer, or continuous phase is represented by μ and ρ. The interface between the two liquids is assumed to be completely described by a single constant parameter, the interfacial tension γ. As shown in figure 1, the geometry of the system is represented by cylindrical coordinates (z, σ, ϕ). We assume that the drop shape and flow field are both axisymmetric; therefore, all quantities are independent of ϕ. The flow fields inside and outside the drop, as well as the drop shape, will be determined using a finite-difference numerical scheme that is a generalization of the method of Ryskin & Leal (1984*a*, *b*).

2.1. *Grid generation*

In order to utilize finite-difference methods, it is necessary to define a coordinate grid, upon which the governing equations can be discretized. For reasons discussed elsewhere (Ryskin & Leal 1984*a*, *b*; Dandy & Leal 1986) we have chosen to use an orthogonal boundary-fitted coordinate grid that is generated numerically. Because of axisymmetry, the grid generation problem takes the form of numerically constructing a discrete set of mapping functions $z(\xi, \eta)$ and $\sigma(\xi, \eta)$, both inside and outside the drop. Briefly, to generate the exterior coordinate system, we use the strong constraint method of Ryskin & Leal (1983, 1984*a*, *b*), which amounts to solving the covariant Laplace equations for z and σ on a unit square in the (ξ, η)-curvilinear coordinate system. The drop surface corresponds to the coordinate line $\xi = 1$, while infinity in the outer domain is $\xi = 0$. It is necessary to also generate a coordinate grid inside the drop, and for this inner problem the coordinate system is spherical in nature, with the point $(\hat{z}, \hat{\sigma}) = (0, 0)$ corresponding to $\xi = 0$. After mapping, the computational domain for both phases will always be a unit square in (ξ, η).

One difficulty which arises in unbounded flow problems is the treatment of conditions at infinity. The two choices available are to either truncate the (z, σ)-domain at some distance from the body, or to perform a coordinate inversion. Grosch & Orszag (1977) compared solutions obtained using coordinate inversion to those obtained via domain truncation for a variety of unbounded domain problems, including Burger's equation, and concluded that mapping will yield more accurate solutions than those obtained with truncation, provided that the solution being sought vanishes rapidly or approaches constant values at infinity. For the present study, we follow Ryskin & Leal (1984*a*, *b*) and use a conformal coordinate inversion of the outer domain:

$$z + \mathrm{i}\sigma = \frac{1}{z^* - \mathrm{i}\sigma^*}, \tag{1}$$

which preserves the orthogonality of the coordinate grid. Thus, rather than map the outer (z, σ) domain directly to the (ξ, η) computational domain, the conformal

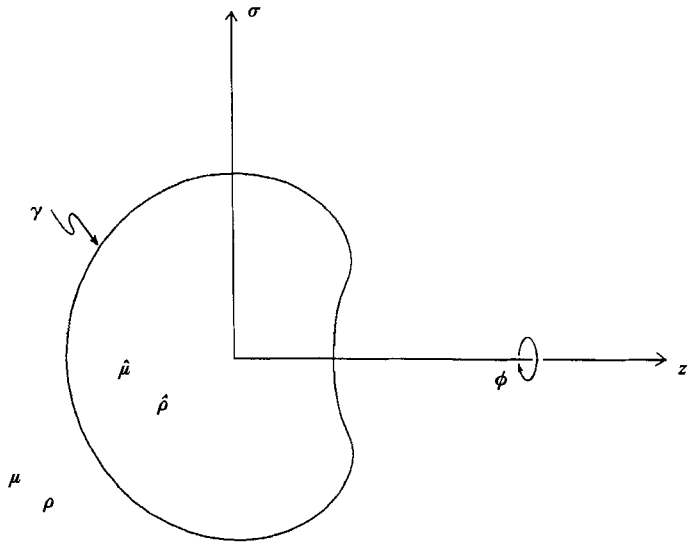

FIGURE 1. Schematic sketch of the problem.

mapping was used to transform the infinite (z, σ) domain to an auxiliary finite domain (z^*, σ^*), which was then mapped to a unit square in the (ξ, η) domain using the numerically generated orthogonal mapping technique. Since the domain inside the drop is finite, it is not necessary to carry out the coordinate inversion; the variables $(\hat{z}, \hat{\sigma})$ are mapped directly onto the (ξ, η) computational domain.

Because of the inherently interesting flow structures which arise at the rear of the drops at larger values of the Reynolds number and Weber number, it is advantageous to use the strong constraint method to generate the coordinate grid in the continuous phase (Ryskin & Leal 1984*a*, *b*). By using this strong constraint method, one can control grid spacing via the distortion function, denoted by $f(\xi, \eta)$. Again, we follow Ryskin & Leal (1984*a*, *b*), and choose $f(\xi, \eta) = \pi\xi(1 - \alpha \cos \pi\eta)$, where $0 \leqslant \alpha < 1$, which results in a grid that is finer at the rear of the drop (near $\eta = 0$) than at the front, and also finer near the drop surface ($\xi = 1$) than at infinity ($\xi = 0$).

There is one critical difference between the mapping problem for the bubble, which requires only one coordinate map external to the bubble surface, and the present problem, which requires both an internal and external coordinate map. If we are to avoid potentially large errors in applying boundary conditions at the drop surface, it is necessary that the two coordinate grids, inside and outside the drop, must match up exactly at the free surface. In order to ensure that this is true, the strong constraint method is used in the outer phase and the weak constraint method is used in the inner phase. In the weak constraint method, complete boundary correspondence is prescribed (similar to other grid generation techniques; see Thompson, Warsi & Mastin 1985), and because of this the distortion function $f(\xi, \eta)$ cannot be specified. The advantage in using the weak constraint method in conjunction with the strong constraint method is that the solution of the strong constraint mapping, namely the position of the free surface $(z(1, \eta), \sigma(1, \eta))$, is used as a boundary condition for the weak constraint method. That is, the strong constraint method generates the grid in the outer domain, with the position of the interface found as part of the solution, and then the weak constraint method is used to generate a grid inside the drop which matches exactly at the interface.

2.2. *Governing equations*

The equations governing the fluid motion and the shape of the drop are the steady-state Navier–Stokes equations and associated boundary conditions, which we state with respect to a frame of reference that is fixed on the drop. In the present work, these equations and boundary conditions are non-dimensionalized using the radius a of an undeformed drop of volume $\frac{4}{3}\pi a^3$ as the characteristic lengthscale, the uniform streaming velocity at infinity U_∞ as a characteristic velocity, and $\frac{1}{2}\rho U_\infty^2$ as the pressure scale. The dimensionless equations then take the form

$$\hat{\boldsymbol{u}}\cdot\nabla\hat{\boldsymbol{u}} = -\frac{1}{2\zeta}\nabla\hat{p} + \frac{2\lambda}{\zeta Re}\nabla^2\hat{\boldsymbol{u}}, \tag{2a}$$

$$\nabla\cdot\hat{\boldsymbol{u}} = 0 \tag{2b}$$

and

$$\boldsymbol{u}\cdot\nabla\boldsymbol{u} = -\tfrac{1}{2}\nabla p + \frac{2}{Re}\nabla^2\boldsymbol{u} \tag{3a}$$

$$\nabla\cdot\boldsymbol{u} = 0. \tag{3b}$$

The pressures p and $\hat{p}$ are dynamic. The hydrostatic pressure contribution will thus appear in the normal stress condition at the drop interface. There are three independent dimensionless groups in these equations: the Reynolds number $Re = 2\rho a U_\infty/\mu$, the density ratio $\zeta = \hat{\rho}/\rho$ and the viscosity ratio $\lambda = \hat{\mu}/\mu$. For some purposes, it is more convenient to identify these three parameters as Re, ζ and an internal Reynolds number $\hat{Re} = Re\,\zeta/\lambda$. The boundary condition at infinity is

$$\boldsymbol{u} \to \boldsymbol{e}_z \quad \text{as} \quad \|\boldsymbol{x}\| \to \infty. \tag{4a}$$

At the drop interface we require continuity of velocity

$$\hat{\boldsymbol{u}} = \boldsymbol{u}, \tag{4b}$$

continuity of stress

$$\boldsymbol{n}\cdot(\boldsymbol{T} - \hat{\boldsymbol{T}}) = \frac{4}{We}(\nabla\cdot\boldsymbol{n})\boldsymbol{n}, \tag{4c}$$

and the kinematic condition

$$\boldsymbol{n}\cdot\hat{\boldsymbol{u}} = \boldsymbol{n}\cdot\boldsymbol{u} = 0. \tag{4d}$$

In (4c) and (4d), $\boldsymbol{T}$ and $\hat{\boldsymbol{T}}$ denote the dimensionless outer and inner stress tensors, respectively, given by

$$\boldsymbol{T} = -p\boldsymbol{I} + \frac{8}{Re}\boldsymbol{\tau}$$

and

$$\hat{\boldsymbol{T}} = -\hat{p}\boldsymbol{I} + \frac{8}{Re}\lambda\hat{\boldsymbol{\tau}},$$

and $\boldsymbol{n}$ is the unit normal to the interface, defined to be positive when pointing into the continuous phase. A fourth independent dimensionless group which appears in the boundary conditions is the Weber number $We = 2\rho a U_\infty^2/\gamma$. It may also be noted that the viscosity ratio λ appears in (4c) as an independent parameter, rather than in the form of an internal Reynolds number, as in (2a). The pressure which appears in the stress balance, (4c), is the total pressure including the hydrostatic contribution. Although this latter term involves the density difference between the two fluids, it does not introduce an additional independent dimensionless parameter because the density difference and the velocity U_∞ are not independent.

Owing to the axisymmetry of the problem, it is convenient to use a stream function–vorticity formulation rather than the primitive variables $\boldsymbol{u}$ and p. To recast the problem, we first take the curl of $(2a)$ and $(3a)$ to obtain an equation in terms of vorticity $\boldsymbol{\omega}$ and velocity $\boldsymbol{u}$. Then we express the velocity components in the general curvilinear coordinate system in terms of the stream function ψ:

$$u_\xi = -\frac{1}{\sigma h_\eta}\frac{\partial \psi}{\partial \eta}, \quad u_\eta = \frac{1}{\sigma h_\xi}\frac{\partial \psi}{\partial \xi},$$

and substitute these into the velocity–vorticity formulation to obtain

$$\mathrm{L}^2(\hat{\omega}\hat{\sigma}) - \frac{\lambda Re}{2\zeta \hat{h}_\xi \hat{h}_\eta}\left[\frac{\hat{u}_\xi}{\hat{h}_\xi}\frac{\partial}{\partial \xi}\left(\frac{\hat{\omega}}{\hat{\sigma}}\right) + \frac{\hat{u}_\eta}{\hat{h}_\eta}\frac{\partial}{\partial \eta}\left(\frac{\hat{\omega}}{\hat{\sigma}}\right)\right] = 0, \tag{5a}$$

$$\mathrm{L}^2\hat{\psi} + \hat{\omega} = 0 \tag{5b}$$

and

$$\mathrm{L}^2(\omega\sigma) - \frac{1}{2}\frac{Re}{h_\xi h_\eta}\left[\frac{u_\xi}{h_\xi}\frac{\partial}{\partial \xi}\left(\frac{\omega}{\sigma}\right) + \frac{u_\eta}{h_\eta}\frac{\partial}{\partial \eta}\left(\frac{\omega}{\sigma}\right)\right] = 0, \tag{6a}$$

$$\mathrm{L}^2\psi + \omega = 0, \tag{6b}$$

where

$$\mathrm{L}^2 \equiv \frac{1}{h_\xi h_\eta}\left[\frac{\partial}{\partial \xi}\left(\frac{f}{\sigma}\frac{\partial}{\partial \xi}\right) + \frac{\partial}{\partial \eta}\left(\frac{1}{f\sigma}\frac{\partial}{\partial \eta}\right)\right].$$

The scale factors of the coordinate system are

$$h_\xi = \left[\left(\frac{\partial z}{\partial \xi}\right)^2 + \left(\frac{\partial \sigma}{\partial \xi}\right)^2\right]^{\frac{1}{2}},$$

$$h_\eta = \left[\left(\frac{\partial z}{\partial \eta}\right)^2 + \left(\frac{\partial \sigma}{\partial \eta}\right)^2\right]^{\frac{1}{2}},$$

and the distortion function is

$$f = \frac{h_\eta}{h_\xi}.$$

The geometric factors L^2, h_ξ, and h_η in each phase are defined in terms of the appropriate coordinate variables.

At large distances from the body the velocity asymptotically approaches the uniform streaming flow $\psi \sim \frac{1}{2}\sigma^2$. To remove this singularity in the stream function we define a modified stream function by subtracting off a function which has the same asymptotic behaviour at large distances and satisfies homogeneous conditions at the other three boundaries. The modified stream function is $\psi^* = \psi - \frac{1}{2}\sigma^2(1-\xi^3)$. The substracted term is the potential-flow solution for a spherical bubble, but it has no simple physical meaning for a drop of arbitrary shape. From the Oseen solution (Proudman & Pearson 1957) we know that ψ^* is bounded at infinity, and because this point is a singular point of the differential equation, boundedness is a sufficient condition for solution (Morse & Feshbach 1953).

The boundary conditions corresponding to (5) and (6) are: along the axes of symmetry,

$$\omega, \psi^*, \hat{\omega}, \hat{\psi} = 0 \quad \text{at} \quad \eta = 0, 1; \tag{7a}$$

at infinity,

$$\psi^*, \omega = 0 \quad \text{at} \quad \xi = 0; \tag{7b}$$

and at the centre of the drop,

$$\hat{\psi}, \hat{\omega} = 0 \quad \text{at} \quad \xi = 0. \tag{7c}$$

At the surface of the drop, there is zero normal velocity when

$$\hat{\psi} = \psi^* = 0 \quad \text{at} \quad \xi = 1, \tag{7d}$$

and continuity of tangential velocity requires that

$$\hat{u}_\eta = u_\eta \quad \text{at} \quad \xi = 1. \tag{7e}$$

The tangential stress balance takes the form

$$\lambda\hat{\omega}_s - \omega_s = 2\kappa_\eta u_\eta(\lambda - 1) \quad \text{at} \quad \xi = 1, \tag{7f}$$

where $\omega_s \equiv \omega(1,\eta)$ and $\hat{\omega}_s \equiv \hat{\omega}(1,\eta)$. Finally, the normal stress balance, (4*c*), is

$$\hat{p} - p + \frac{8}{Re}\left[\frac{\lambda}{\hat{\sigma}\hat{h}_\eta}\frac{\partial}{\partial\eta}(\hat{\sigma}\hat{u}_\eta) - \frac{\partial}{\sigma h_\eta}\frac{\partial}{\partial\eta}(\sigma u_\eta)\right] = \frac{4}{We}(\kappa_\eta + \kappa_\phi)|_{\xi=1}, \tag{7g}$$

where the difference in pressure is given by

$$\hat{p} - p = -\tfrac{3}{4}C_D z - \zeta\hat{u}_\eta^2 + u_\eta^2 + \frac{4}{Re}\left[\lambda\int\frac{\hat{f}}{\hat{\sigma}}\frac{\partial}{\partial\xi}(\hat{\sigma}\hat{\omega})\,\mathrm{d}\eta + \int\frac{f}{\sigma}\frac{\partial}{\partial\xi}(\sigma\omega)\,\mathrm{d}\eta\right] + C_1|_{\xi=1}.$$

The constant C_1 is determined in the present solutions by requiring the drop to conserve volume.

$$C_D = 2\int_0^1 \left(\tau_{\xi\xi}\frac{\partial\sigma}{\partial\eta} - \tau_{\xi\eta}\frac{\partial z}{\partial\eta}\right)\sigma\,\mathrm{d}\eta,$$

with

$$\tau_{\xi\xi} = u_\eta^2 + \frac{4}{Re}\left[\int^\eta \frac{f}{\sigma}\frac{\partial}{\partial\xi}(\sigma\omega)\,\mathrm{d}\eta - \frac{2}{\sigma h_\eta}\frac{\partial}{\partial\eta}(\sigma u_\eta)\right],$$

$$\tau_{\xi\eta} = \frac{4}{Re}(2\kappa_\eta u_\eta - \omega),$$

and the normal curvatures are

$$\kappa_\eta = \frac{1}{h_\eta^3}\left(\frac{\partial z}{\partial\eta}\frac{\partial^2\sigma}{\partial\eta^2} - \frac{\partial^2 z}{\partial\eta^2}\frac{\partial\sigma}{\partial\eta}\right)\Big|_{\xi=1}$$

and

$$\kappa_\phi = -\frac{1}{\sigma h_\xi}\frac{\partial\sigma}{\partial\xi}\Big|_{\xi=1}.$$

The incorporation of these boundary conditions into the numerical computatons will be discussed in the next section.

2.3. *Details of the numerical scheme*

The numerical scheme used to solve the partial differential equations is the ADI method of Peacemann & Rachford (1955). An artificial time dependence is embedded in (5*a*, *b*) and the Laplace equations governing the mapping, and the PDE's are approximated using second-order centred finite differences (see, for example, Ryskin & Leal 1984*a*, *b*). Although (5*a*) and (5*b*) are coupled, and the two mapping equations are coupled through the distortion function f, each set of equations is solved successively rather than simultaneously at each iteration or time step.

The homogeneous Dirichlet conditions (7*a–d*) do not introduce any additional terms in the tridiagonal system generated by applying ADI and, further, they are strong conditions in the sense that they 'tie down' the values of the unknown vorticity at three of the four boundaries of the domain. The remaining three boundary conditions – continuity of tangential velocity and the tangential and

normal stress balances – must somehow be used to specify the three remaining unknown quantities: the interface shape, and the interface vorticity values $\hat{\omega}(1,\eta)$ and $\omega(1,\eta)$. For application as boundary conditions, it is *not* sufficient to use (7*e*) and (7*f*) as written; the numerical scheme requires explicit values for $\hat{\omega}_s$ and ω_s. Instead, we use an approach based on a method developed by Dorodnitsyn & Meller (1968) and Israeli (1970), and described elsewhere (Ryskin 1980). Briefly, the facts that (i) the strength of the vorticity sheet at the interface is proportional to the velocity difference and (ii) $\hat{u}_\eta(1,\eta) \neq u_\eta(1,\eta)$ until numerical convergence is reached are both used to explicitly specify $\hat{\omega}(1,\eta)$ and $\omega(1,\eta)$ at each ADI step. That is, until continuity of tangential velocity is satisfied, the local vorticity is adjusted proportionally to the magnitude of the velocity jump, which itself is proportional to the strength of the corresponding vortex sheet at the interface. The diffusion and convection of vorticity leads to a smoothing of the velocity discontinuity. Equations (7*a–f*) are sufficient to obtain solutions to the flow equations for ψ^*, $\hat{\psi}$, ω and $\hat{\omega}$. The position of the interface is then updated using the normal stress balance, (7*g*), in a manner analogous to Ryskin & Leal (1984*a*, *b*). Finally, the unknown constant C_1 in the pressure expression is determined by requiring that the drop conserve volume each time the interface position is adjusted.

All calculations were done on a CRAY XM-P/24. The code was vectorized wherever possible. In fact, with the exception of one loop in the entire program, all of the inner loops were vectorized. Even though the solution of the tridiagonal system arising from the ADI scheme is recursive in nature, it is possible to reverse the order of the loops and thus make the inner loop vectorizable. Owing to the extreme under-relaxation needed in employing the normal stress balance to update the interface shape at the end of each iteration, a fairly large number of iterations were required, particularly at the larger Weber numbers. The difficulty in obtaining convergence at large values of *We* was also encountered by Ryskin & Leal (1984*a*, *b*). In fact, these problems with the numerical method have led us to formulate a Newton's method scheme for solving free-surface flow problems (Dandy & Leal 1989). The number of iterations needed here was usually in the range 1000–7500, depending on the Weber number, and the corresponding CPU time required on the CRAY was roughly 15 to 120 s. Two criteria were used to determine when the solution was fully converged: the maximum norm of the relative difference between the inner and outer velocities and the maximum norm of the absolute error in evaluating (7*g*) both had to be less than 10^{-3}. We found that if these two convergence criteria were satisfied, the governing equations were also satisfied to within acceptable tolerances. Specifically, the maximum norms of the residuals of (6) were always $o(10^{-4})$.

Solutions were obtained by choosing values for λ, ζ, *Re* and *We* and marching along one of the parameter branches while holding the other three fixed. In this manner, the solution at a particular set of parameter values were used as the initial guess for an incremental change in one of the four parameters.

To explore solution behaviour as a function of the parameter space, we divided the problem into three parts. First, we examine the effect of changing Reynolds number and Weber number (as would happen if the diameter of the undeformed drop were changed) while holding the fluid properties λ and ζ fixed. Second, the viscosity ratio λ and the density ratio ζ are varied independently while *Re* and *We* are held fixed. Finally, the solutions for low $Re\,(<1)$ and high $Re\,(>100)$ are compared, where appropriate with the existing asymptotic solutions for high and low Reynolds number, and also with experimental observations.

3. Results and discussion

3.1. *Numerical results*

In order to illustrate the effects of variations in Re and We, we begin with a series of solutions with the density ratio and viscosity ratio fixed at representative $O(1)$ values of $\zeta = 0.91$ and $\lambda = 4$, respectively. Although these specific values are rather arbitrary, they are chosen for present purposes with the general aim of having a drop viscosity that is large enough to expose interesting flow behaviour (recirculating wakes) for moderate Reynolds numbers where solution accuracy is not an issue. In general, the qualitative dependence of the solutions on Re and We, illustrated below, was invariant to λ and ζ, though the details of drop shape and the flow fields were different. We shall examine some of these differences later in this section.

Figures 2 and 3 show our results for the drop shape and the flow field at Reynolds numbers of 2 and 10 for the values of λ and ζ mentioned above, and several values of We. Table 1 contains the corresponding values of the drag coefficient. (Values of C_D for all solutions obtained in this work are displayed in table 1.) For fixed values of λ, ζ, and Re, the shapes shown in figure 2 become more deformed with increasing We (or decreasing surface tension), tending towards a spherical cap shape at the higher values of the Weber number. The stream function plots in figure 3 show that at the lower values of Re the external flow, moving from left to right, induces the motion of a single, primary vortex inside the drop. The results for shape and external flow are qualitatively similar to those found by Ryskin & Leal for gas bubbles at the same values of Reynolds number and Weber number. However, at any particular Re and We the drop is less deformed than the bubble.

In addition to the streamlines, we also show the corresponding vorticity fields in figure 3 for $Re = 10$. The values of vorticity are largest near the top of the drop where, incidentally, curvature is the highest, and smallest on the axes of symmetry, where the value is zero. Because of the orientation of our coordinate system, all values of vorticity shown, for example at $Re = 10$, $We = 0.5$, are negative. For small values of Re and We, such as $Re = 0.5$, $We = 0.5$, the internal streamlines resemble Hill's spherical vortex, that is, a fore–aft symmetric recirculating ring, and the vorticity is a function of $\hat{\sigma}$ only, so that lines of constant vorticity are horizontal. As the Reynolds number is increased, for example to 10 as in figure 3, the internal vortex is gradually shifted towards the front of the drop. The lines of constant vorticity than deform in the interior, bending upwards as they approach the surface at the rear of the drop. Finally, when the drop becomes sufficiently deformed, for $We \geqslant 4$, a region of positive vorticity appears, both inside and outside, at the rear of the drop. In a general sense, the appearance of a region of vorticity of opposite sign at the rear of the drop is no surprise. For example, a very similar region is found for both a solid sphere and a deformable bubble at high enough Reynolds numbers. Indeed, Lighthill (1986) has presented a cogent, qualitative argument to explain the change in sign of the vorticity at the rear of a solid body, and a similar argument can be constructed for a bubble or drop. The unusual feature of the solutions in figure 3 is that the change in sign of the surface vorticity is not accompanied by the appearance of a detachment point and recirculating wake. For either a solid particle or a bubble (i.e. a void with a zero shear stress condition at the surface), a change in sign of the vorticity at the boundary is necessarily accompanied by the appearance of an attached circulating wake. In fact, the point where $\omega_s = 0$ corresponds precisely to the detachment point in both of these cases. For a drop, this is not necessarily true as evidenced by the solutions in figure 3. We shall return to discuss the wake

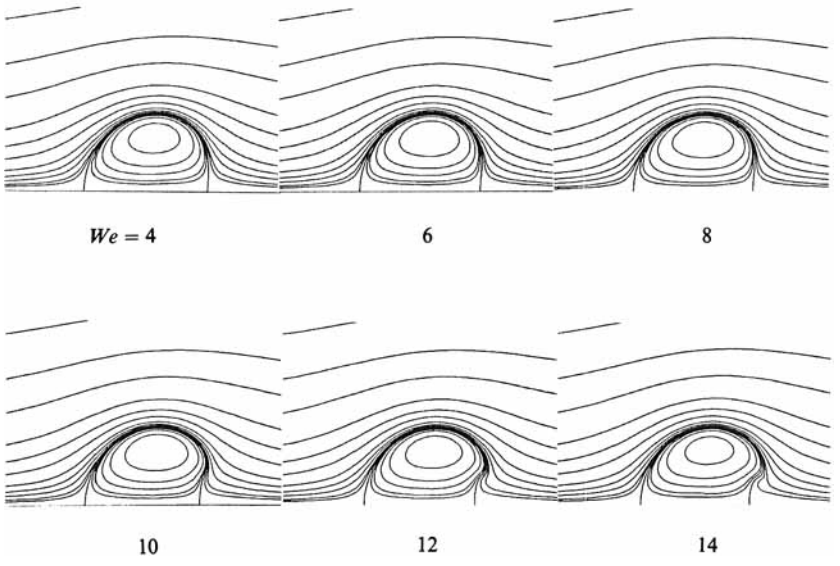

FIGURE 2. Drop shapes and streamlines at various values of We for $Re = 2$, $\zeta = 0.909$, and $\lambda = 4$.

structure and vorticity distribution in more detail shortly; however, it is advantageous to first examine solutions for other, larger values of Re.

Thus, we show two additional sets of solutions for the same values of λ and ζ as above, but for $Re = 60$ and 100, respectively, with Weber number varying up to a maximum value $We \leqslant 8$. The solutions for $Re = 60$ are shown in figure 4, while those for $Re = 100$ are given in figure 5. Comparing the results with the solutions in figure 3 for $Re = 10$, we see important qualitative changes in both the drop shape and in the flow downstream of the drop. The main change in shape with increase of Re is that the drop becomes increasingly flattened at the front. Essentially, as Re increases the drop deformation is increasingly due to dynamic pressure forces, rather than viscous stresses, and there is thus a tendency for all regions near stagnation points to be pushed inward owing to the local maximum in pressure which exists at these points. Insofar as this trend is concerned, the solutions for a relatively viscous drop ($\lambda = 4$) behave in a manner that is qualitatively similar to rising gas bubbles as reported earlier by Ryskin & Leal (1984*a*, *b*). It should be noted, however, that this tendency to flatten near stagnation points of the external flow is counteracted to a considerable extent for finite values of $\zeta = 0.91$, as considered here, by the fact that the same points are also stagnation points for the internal flow, and thus correspond to internal pressure maxima too.

The most striking flow feature for both $Re = 60$ and 100 is the detached recirculating wake. This detached wake for the liquid drop is in marked contrast to the well-known attached wakes which exist on both bubbles and voids (Ryskin & Leal 1984*a*, *b*; Miksis, Vanden-Broeck & Keller 1981), and solid particles (Taneda 1956; Nisi & Porter 1923; Rimon & Cheng 1969). However, as noted earlier, unattached wakes have previously been observed experimentally and predicted numerically for streaming flow past viscous spherical drops (Garner & Tayeban 1960; Rivkind & Ryskin 1976; LeClair 1970; Oliver & Chung 1987). Although the surface curvature for the drops at a given Re and We is smaller than for the gas bubbles of Ryskin & Leal (1984*a*, *b*), sufficient vorticity can still be produced to lead to eddy

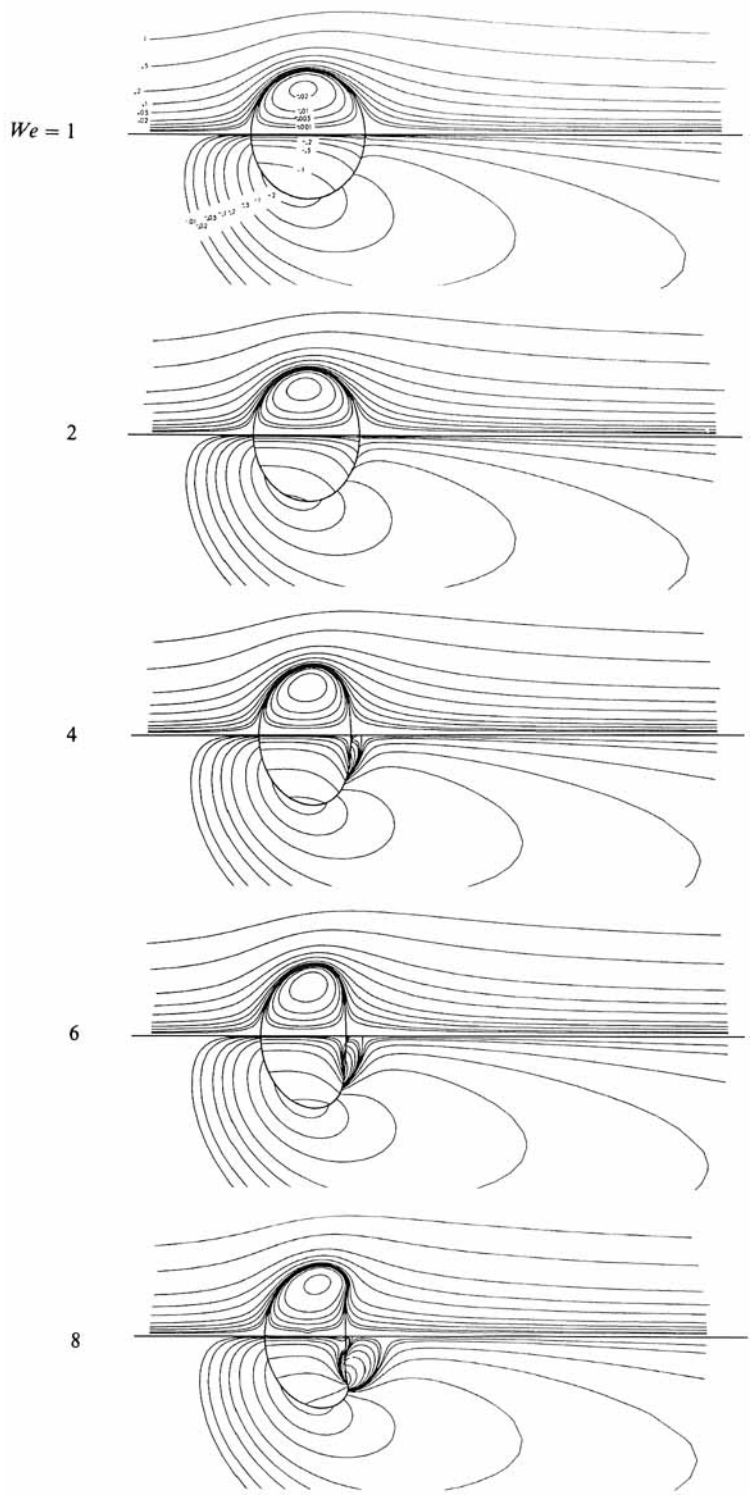

FIGURE 3. Vorticity lines and streamlines for several values of We for $Re = 10$, $\zeta = 0.909$, and $\lambda = 4$; $|\psi| \geqslant 10^{-3}$ and $|\omega| \geqslant 10^{-2}$.

Re	We	λ	ζ	C_D	Re	We	λ	ζ	C_D
0.5	0.5	1.33	0.91	42.3		2	1	0.1	0.998
	1	1.33	0.91	42.5		2	0.5	0.91	0.890
	2	1.33	0.91	42.6		2	0.01	0.1	0.757
	4	1.33	0.91	42.8	60	4	100	1000	1.61
2	0.5	4	0.91	13.92		4	100	100	1.66
	1	4	0.91	14.05		4	100	10	1.67
	1	0.01	0.91	10.11		4	4	0.91	1.43
	1	0.01	0.1	10.11		4	1.33	0.91	1.22
	2	4	0.91	14.20		4	1	2	1.15
	4	4	0.91	14.38		4	0.01	0.1	1.04
	6	4	0.91	14.52		6	10	0.91	1.51
	8	4	0.91	14.71		6	4	0.91	1.65
	10	4	0.91	14.95		8	4	0.91	0.185
	12	4	0.91	15.09	80	0.5	4	0.91	1.08
	14	4	0.91	15.23	100	0.5	4	0.91	0.958
5	1	1.33	0.91	5.80		1	2	0.91	0.856
	2	1.33	0.91	5.88		2	4	0.91	1.00
	4	1.33	0.91	6.12		4	∞	—	1.31
10	0.5	4	0.91	3.96		4	1000	0.91	1.30
	1	4	0.91	4.01		4	500	0.91	1.29
	1	0.01	0.91	2.68		4	200	2000	1.31
	1	0.01	0.1	2.69		4	200	500	1.29
	2	4	0.91	4.10		4	200	1000	1.29
	4	4	0.91	4.28		4	100	0.91	1.29
	6	4	0.91	4.42		4	50	20	1.28
	8	4	0.91	4.88		4	50	0.91	1.28
20	1	100	1000	2.72		4	10	0.91	1.21
	2	100	1000	2.74		4	4	0.91	1.10
	4	100	1000	2.80		4	2	0.91	0.990
	6	100	1000	2.85		4	1	0.91	0.919
40	0.5	4	0.91	1.62		6	4	0.91	1.21
60	0.5	4	0.91	1.27		8	4	0.91	1.30
	0.5	0.01	0.001	0.589	150	1	2.5	0.91	0.78
	1	0.01	0.91	0.660	200	1	2.5	0.91	0.68
	1	0.01	0.1	0.664	250	1	2.5	0.91	0.61
	2	10	0.91	1.35	275	1	2.5	0.91	0.58
	2	4	0.91	1.31	300	1	2.5	0.91	0.56
					350	1	2.5	0.91	0.51

TABLE 1. Values of Re, We, λ and ζ, and the corresponding values of drag coefficient C_D for all solutions obtained

formation because vorticity is also generated via the no-slip condition at the interface. It is worth noting, in this regard, that the maximum dimensionless surface vorticity for both $Re = 60$ and 100 has a value of approximately 7 when a closed-streamline wake first appears, and this value is similar to the maximum surface vorticity when a closed-streamline wake first appears for both a gas bubble and a solid sphere at similar Reynolds numbers. We shall have more to say regarding this later.

An immediate question is whether we can understand the occurrence of a detached wake in the case of a viscous drop, when recirculating wakes behind a solid body or

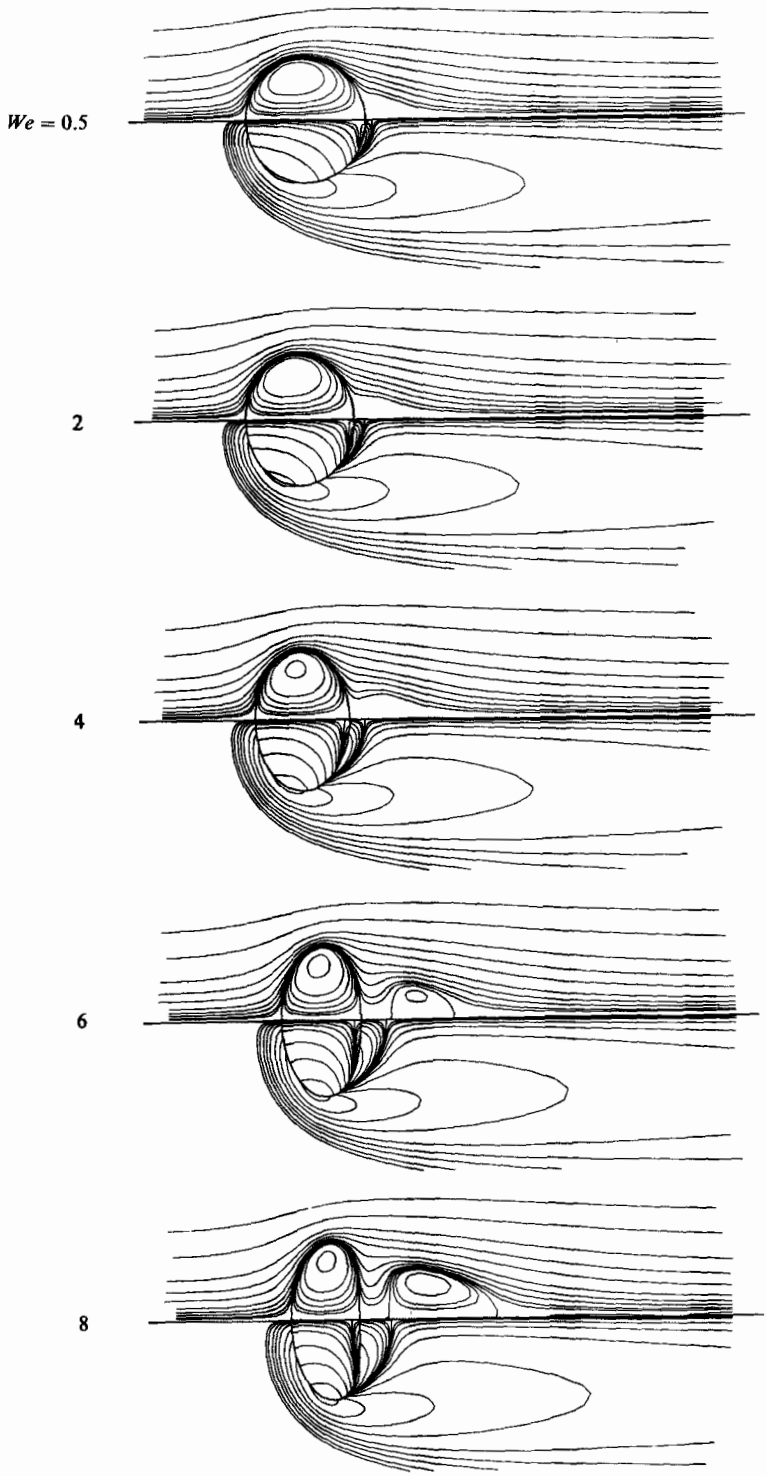

FIGURE 4. Stream function $|\psi| \geqslant 10^{-3}$ and vorticity $|\omega| \geqslant 10^{-2}$ plots for $\lambda = 4$ and $\zeta = 0.91$ as a function of We for $Re = 60$.

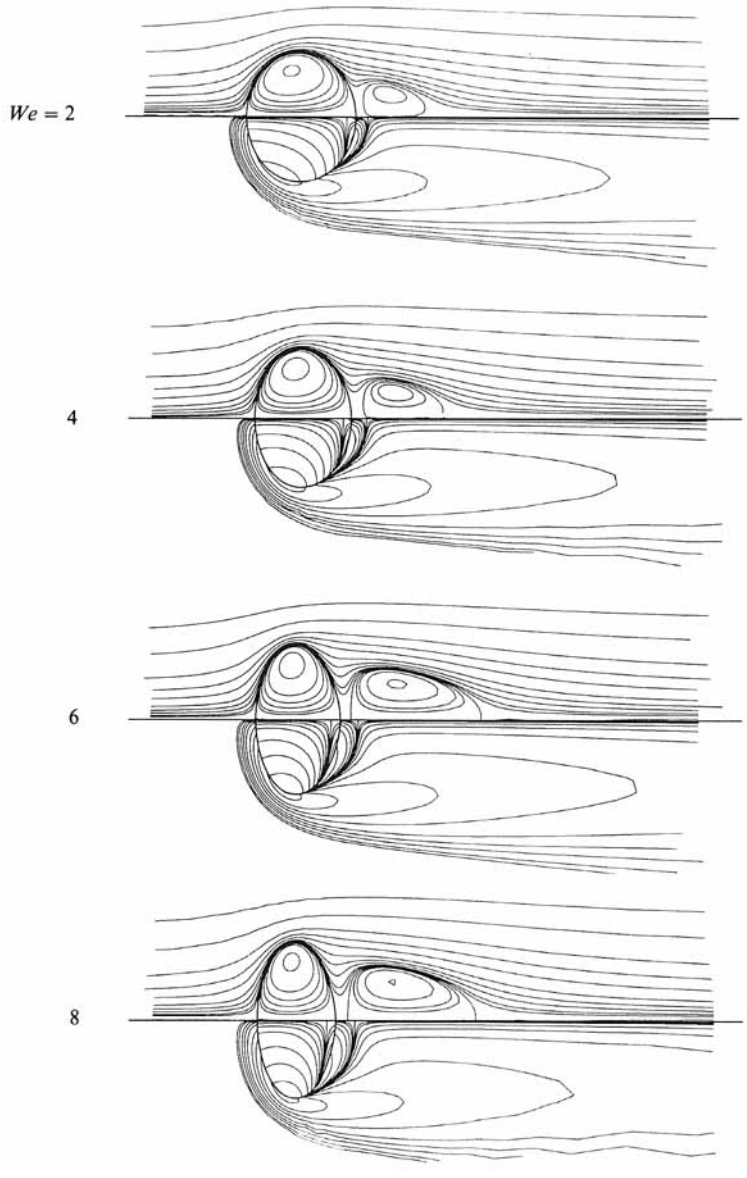

FIGURE 5. Stream function $|\psi| \geqslant 10^{-3}$ and vorticity $|\omega| \geqslant 10^{-2}$ plots for $\lambda = 4$ and $\zeta = 0.91$ as a function of We for $Re = 100$.

a bubble/void with $\hat{\mu} = \hat{\rho} = 0$ are attached. Unfortunately, we have not been entirely successful in trying to resolve this basic question. The best that we can do at this time is to suggest that there are plausible physical arguments which provide some insight into the occurrence of a detached wake, and show that such a flow structure does not violate any of the physical conditions of the problem.

Let us begin with the last point – namely, to show that a detached wake is consistent with the boundary conditions for a drop. For this purpose, it is useful to contrast the flow structure for a drop with that obtained theoretically and experimentally for solid bodies and bubbles/voids, where recirculating wakes are attached to the body surface. We have previously expressed the view, based upon a

numerical study of the wake structure behind a bubble/void (Dandy & Leal 1986; Leal 1989), that recirculating wakes behind any body at moderate Reynolds numbers, $O(10^2)$, should be viewed as resulting from the accumulation of vorticity generated upstream on the body surface. Such a view is consistent with the empirical observation that the maximum value of surface vorticity must exceed a minimum threshold level (dependent upon Re) before a recirculating wake appears, which is approximately independent of whether the boundary condition at the surface is no slip, zero shear stress or an intermediate condition. It is also motivated by the theoretical and experimental observation of closed wakes behind a bubble/void at finite Reynolds number, even though both boundary-layer analysis and numerical solutions indicate no 'separation' or recirculating wakes at larger Reynolds numbers. Thus, in general, if the maximum vorticity at a body surface becomes sufficiently large, we can anticipate the existence of a closed-streamline eddy behind the body. By itself, however, this tells us nothing about whether the eddy will be attached or detached. Indeed, though our experience with solid bodies may seem to suggest that such wakes should always be attached, experiments carried out many years ago have already shown that a detached wake can be generated easily even for a solid body simply by blowing fluid out through the rear surface of the body ('base bleed') (Leal & Acrivos 1969). In order to predict attachment or detachment, we need additional information.

For the solid without base bleed and for the bubble/void, the necessary information can be obtained by considering the vorticity distribution at the body surface. We have already indicated that Lighthill has provided a strong argument to suggest that the surface vorticity for solid bluff bodies should change sign, and generalization of this argument plus numerical evidence shows that this is a general feature of streaming flows regardless of whether the body is a solid, a bubble/void or a drop. However, once we concede that the surface vorticity changes sign, it can be proven that a region of flow immediately adjacent to the body surface must undergo flow reversal for either a solid body or a bubble/void. For the solid, the surface vorticity is proportional to the normal derivative of the tangential velocity component. Hence, if ω_s changes sign, the velocity gradient must change sign and thus, since $\boldsymbol{u} \equiv 0$ on the surface, the direction of tangential motion adjacent to the boundary must reverse at the point $\omega_s = 0$. Although this does not prove that the reverse flow near the boundary is part of the primary vortex, it is implausible to suggest otherwise. For a bubble or void, the existence of a change in sign for ω_s also guarantees existence of flow reversal at $\omega_s = 0$, and, presumably, attachment of the recirculating eddy. To see this, we can examine the condition of zero tangential stress, expressed in terms of the vorticity (this condition can be obtained directly by setting $\lambda = 0$ in $(7f)$,

$$\omega_s - 2\kappa_\eta u_\eta = 0.$$

Provided κ_η is non-zero, we can see that a point where $\omega_s = 0$ corresponds to a point where the interface velocity changes sign. Again, a change in sign for ω_s signals a detachment point on the bubble surface and the implication of an attached primary eddy.

For the drop, however, the situation is not so simple. In this case, the relevant conditions are continuity of tangential velocity and continuity of tangential stress, i.e. $(7f)$,

$$\lambda\hat{\omega}_s - \omega_s = 2\kappa_\eta u_\eta(\lambda - 1)|_{\xi=1}.$$

Now, a change in sign of the vorticity in the outer fluid, i.e. $\omega_s = 0$, does not signal the existence of a detachment point where $u_\eta = \hat{u}_\eta = 0$ unless $\lambda\hat{\omega}_s$ changes sign at

precisely the same point as ω_s. However, we have not been able to demonstrate that this should be expected, nor is it seen to occur in the numerical solutions that we have examined so far. An exception, of course, is $\lambda \equiv 1$ where continuity of tangential stress requires

$$\omega_s = \hat{\omega}_s.$$

However, in this case the tangential stress condition is satisfied for any u_η and there is no reason to expect that $\omega_s = \hat{\omega}_s = 0$ should correspond to $u_\eta = 0$. Indeed,

$$\omega_s = \kappa_\eta u_\eta - \frac{1}{h_\xi}\frac{\partial u_\eta}{\partial \xi},$$

so that $\omega_s = 0$ implies only a geometry-dependent relationship between u_η and $\partial u_\eta/\partial \xi$. From the preceding arguments, we conclude that a change in sign of ω_s (which may be expected according to the Lighthill argument for sufficiently large Re and/or We) does not imply the existence of a detachment point on the drop surface. Clearly, this does not prove that a detachment point will not occur, but there is no way to prove that the necessary condition $\lambda\hat{\omega}_s - \omega_s = 0$ will ever occur and the numerical results obtained in the present study never exhibited an attached recirculating flow.

The preceding arguments essentially show that there is no obvious reason, based upon the boundary conditions, to anticipate that a recirculating wake will either exist or be attached, even if the vorticity on a drop surface changes sign. A stronger question is whether a detached wake could have been predicted *a priori*, or at least anticipated on plausible physical grounds. The best that we can do with this important question is to indicate that a flow structure consisting of a single eddy inside the drop and a single attached eddy outside is implausible. The situation is sketched in figure 6(*a*). Inside the drop, very close to the surface, the fluid is moving in a clockwise direction, toward the rear stagnation point, while the outer fluid in the recirculating region of the wake is moving in the opposite direction. The implication is that u_η will be non-zero on the surface, all the way from the front stagnation point to the detachment point, but then be identically zero from the detachment point to the rear stagnation point. The detached wake configuration, sketched again in figure 6(*b*), is one way to avoid this implausible situation. However, it is not a unique resolution. Another possibility is that the external eddy could be attached so that u_η changes sign on the drop surface, but then there must exist a second internal eddy with the same detachment point as sketched in figure 6(*c*). There is no obvious way to determine *a priori* which of the two configurations 6(*b*) or 6(*c*) should occur (or even whether one of an indefinite number of other self-consistent configurations might appear). In fact, a double internal eddy structure has been observed in both numerical calculations (Rivkind & Ryskin 1976; LeClair *et al.* 1972), and experiments (Pruppacher & Beard 1970), but only for $Re \gg 1$ and $\zeta \gg \lambda \gg 1$, which corresponds roughly to a mercury droplet or perhaps a water droplet falling through air. The present results indicate that the detached wake will occur for other ranges of the dimensionless parameters (though some caution must be used in extrapolation to parameter ranges that are far from those that we have actually examined).

All of the results discussed so far were obtained by varying We with the other parameters held fixed. Here, we consider the effect of viscosity ratio. In particular, in figure 7 we present results for the case $Re = 100$, $We = 4$, $\zeta = 0.91$ and $1 \leqslant \lambda \leqslant 1000$. An alternative view of these results is in terms of fixed values for the internal Reynolds number $\hat{Re}$ decreasing from 90 down to 0.09. One consequence of increasing λ (or decreasing $\hat{Re}$) is a slight decrease in deformation. A more dramatic and interesting effect of increasing λ is that the wake becomes larger in size, roughly

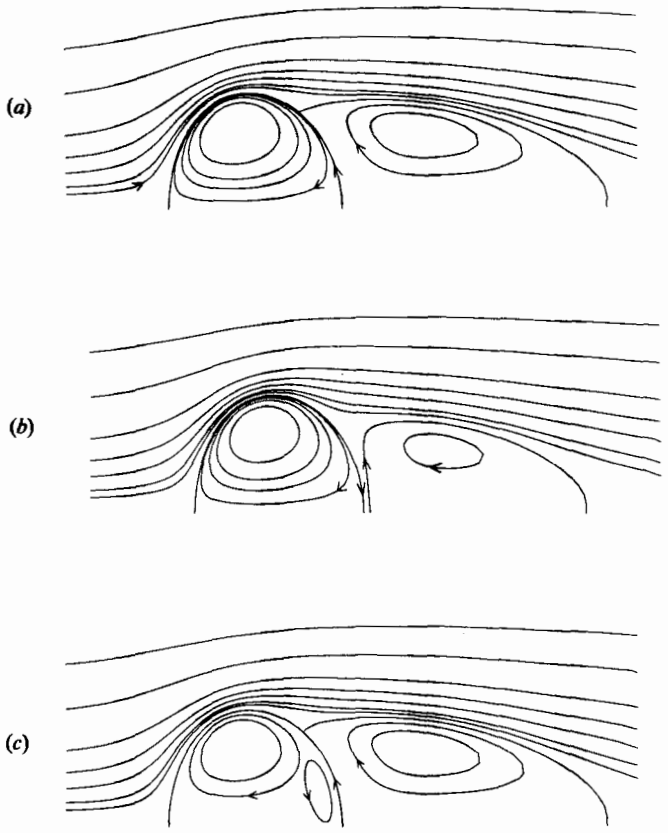

FIGURE 6. (*a*) Schematic of a hypothetical flow field (with arrows indicating the direction of flow) for the case of a liquid drop with an attached wake. (*b*) Schematic for the flow field for the case of a liquid drop with a detached wake. (*c*) Schematic of the flow field for liquid drop with attached wake and secondary interior recirculating vortex.

in proportion to the increase in the surface vorticity as the no-slip condition becomes a more effective source of vorticity. We have seen that there are two mechanisms for producing vorticity at the surface of the drop: curvature and the no-slip condition. The results in figure 7 demonstrate that the no-slip mechanism is a more efficient source of vorticity than curvature at this Re, We and ζ because, as λ increases, the curvature source decreases owing both to the slight decrease in curvature and to the sharp decrease in surface velocity, while the no-slip mechanism increases.

It may also be noted that the strength of the flow inside the drop becomes correspondingly smaller as the viscosity ratio becomes larger, and the detached wake moves in closer to the body. Indeed, we find that

$$\max_j |u_\eta(1, \eta_j)| \propto \lambda^{-1}.$$

When the viscosity ratio λ is $O(1)$, the velocity at the surface of the drop is of the same magnitude as the characteristic velocity, U_∞. However, as λ rises the surface velocity falls, and the flow inside the drop becomes weaker. The fact that the wake simultaneously moves closer to the drop would seem to support the idea that it exists in a detached state because it is forced to do so by the internal flow. The flow fields

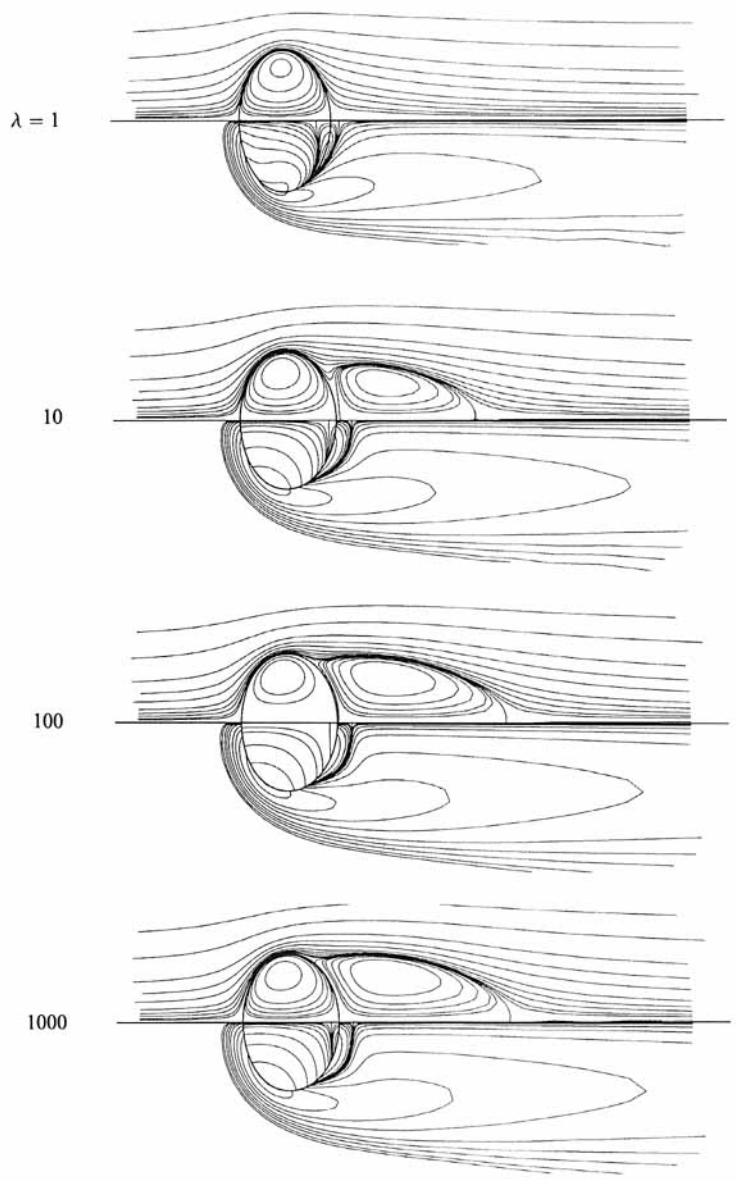

FIGURE 7. Stream function $|\psi| \geqslant 10^{-3}$ and vorticity $|\omega| \geqslant 10^{-2}$ plots of $Re = 100$, $We = 4$ and $\zeta = 0.91$ as a function of λ. For the last plot, $\lambda = 1000$, the inner stream function and vorticity values are $|\hat{\psi}| \geqslant 10^{-5}$ and $|\hat{\omega}| \geqslant 10^{-4}$.

in figure 7 show that at the lower viscosity ratios the wake is not only smaller than at the larger λ (since less vorticity is being produced at the interface), but it is also farther away from the body owing to the increased strength of the flow inside the drop.

The surprising fact is that the wakes at even the highest vorticity ratios considered in the present study, i.e. $\lambda = 100$ and $\lambda = 1000$, are actually still detached from the drop surface. However, this is easily demonstrated by examining the signs of the velocity at the interface. The limit $\lambda \to \infty$ can be regarded as a solid particle and the

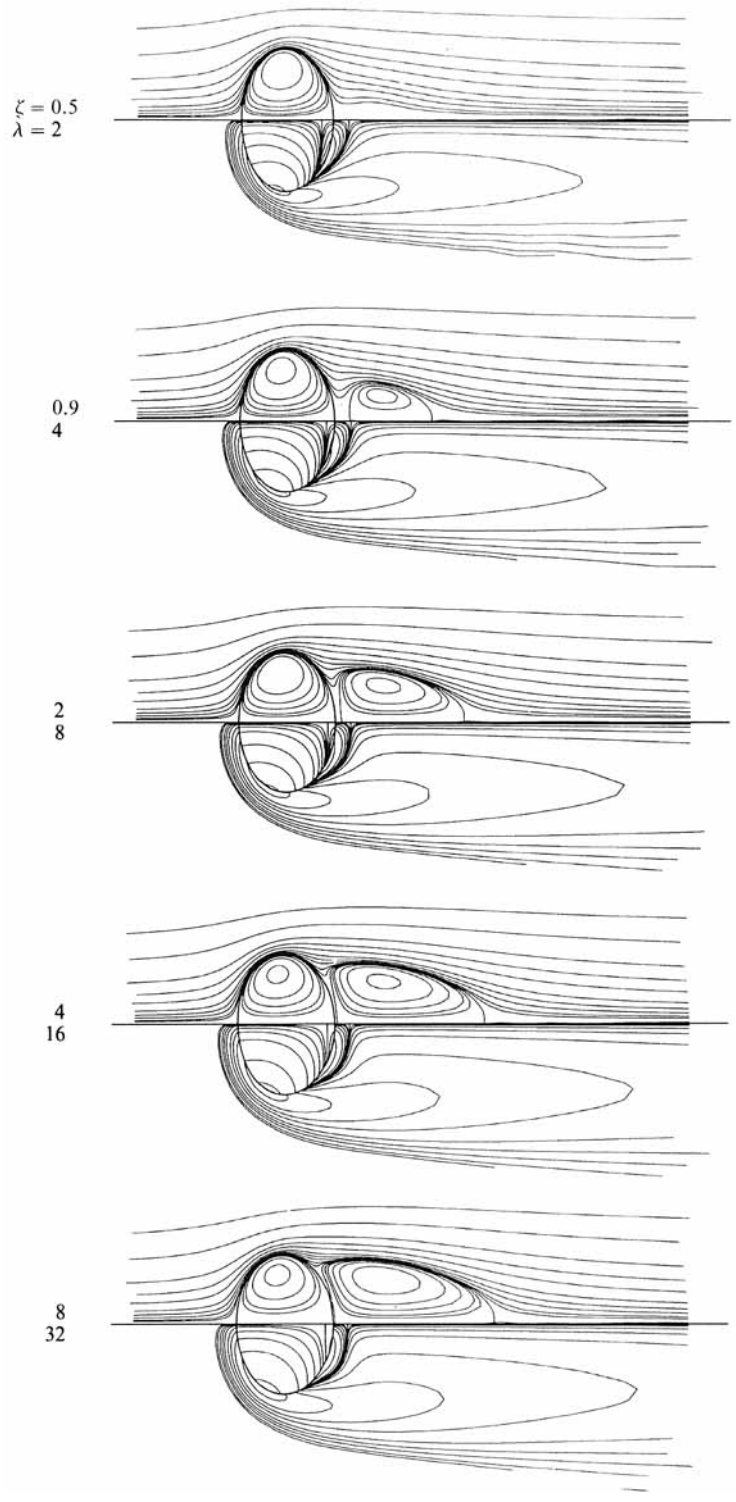

FIGURE 8. Stream function $|\psi| \geqslant 10^{-3}$ and vorticity $|\omega| \geqslant 10^{-2}$ plots for $Re = 100$ and $We = 4$ as a function of $\zeta/\lambda = 0.25$.

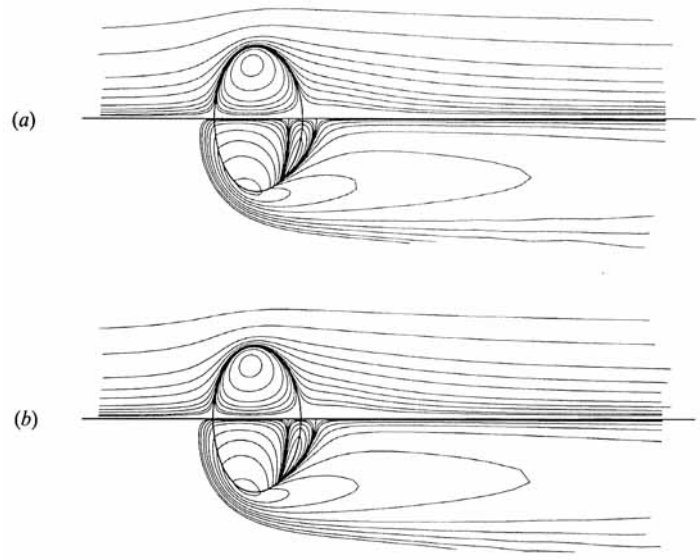

FIGURE 9. Stream function $|\psi| \geqslant 10^{-3}$ and vorticity $|\omega| \geqslant 10^{-2}$ plots for $Re = 100$, $We = 4$ and $\lambda = 1$: (*a*) $\zeta = 0.1$; (*b*) $\zeta = 0.01$.

wake behind such a body will be attached (see, for example, Masliyah 1970; Nakamura 1976). The calculations here show that as λ increases the wake moves closer to the drop, but up to $\lambda = 1000$ it is still not attached. On this basis, it appears that the limit $\lambda \to \infty$ is singular insofar as wake attachment is concerned.

Although Re was held fixed to obtain the results shown in figure 7, the interior Reynolds number actually decreased as λ increased. To investigate the effect of varying λ and ζ for fixed inner and outer Reynolds numbers, we did a series of calculations for $Re = 100$ and $We = 4$ with various values of ζ and λ, holding their ratio fixed at 0.25 (i.e. $\zeta/\lambda = 0.25$, and thus the inner Reynolds number was 25 in all cases). The results of these calculations are shown in figure 8. It is noteworthy that the solutions look very similar to those in figure 7, in spite of the fact that λ and ζ are both increased in figure 8, whereas only λ was increased in figure 7. Indeed, as λ and ζ are increased, the drop becomes less deformed, the surface velocity slows down in proportion to λ^{-1}, and the wake grows larger and moves closer to the rear of the drop. The conclusion from comparing these results with figure 7, is that neither the internal Reynolds number nor the density ratio ζ plays an important role in determining the flow field, at least in the range of parameters represented by figures 7 and 8.

This is not really surprising since ζ appears only indirectly in the boundary conditions through the pressure, whereas the vorticity ratio λ appears in the viscous terms of both the tangential and normal stress balances. This observation has been confirmed by other numerical computations, particularly those of Rivkind & Ryskin (1976).

This conclusion can be further corroborated by displaying some results in which λ is held fixed and ζ varied. Two such sets of results are shown in figures 9 and 10. In figure 9, we show results for $Re = 100$, $We = 4$, $\lambda = 1$ and two values of $\zeta = 0.1$ and 0.01. Together with the first result in figure 7, for $\zeta = 0.5$, we see that a factor of 50 change in the magnitude of the density ratio produces only a slight change in drop shape, and flow field, again supporting the conclusion stated previously of only very

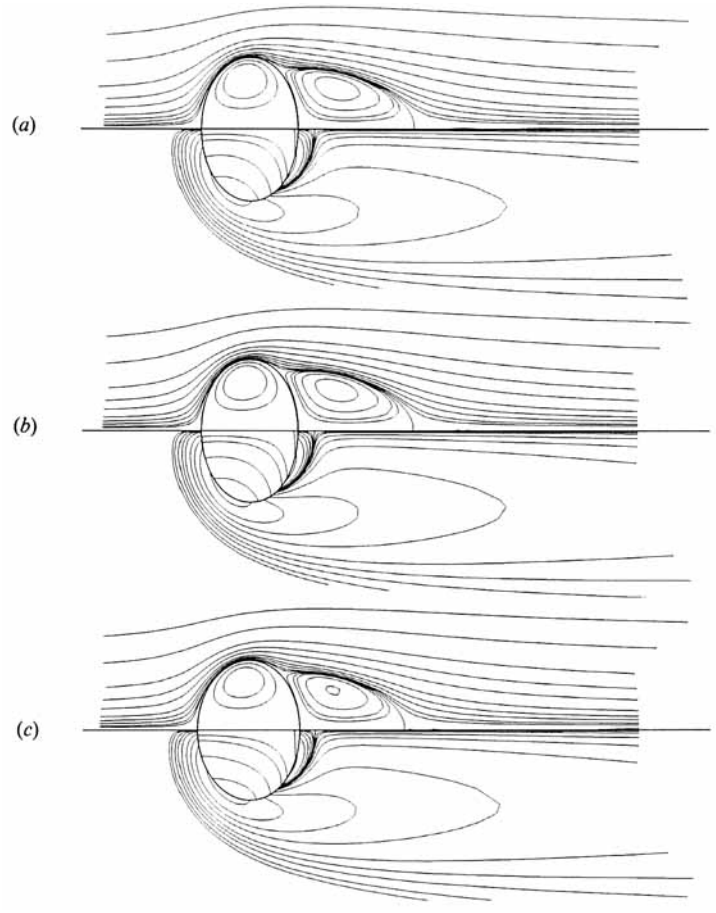

FIGURE 10. Stream function $|\psi| \geqslant 10^{-3}$ and vorticity $|\omega| \geqslant 10^{-2}$ plots for $Re = 60$, $We = 4$ and $\lambda = 100$: (*a*) $\zeta = 10$; (*b*) $\zeta = 100$; (*c*) $\zeta = 1000$.

weak dependence of the flow behaviour on ζ. However, these results consider only small density ratios, and small internal Reynolds numbers, $\hat{R}e = 10$ and 1, respectively, for figures 9(*a*) and 9(*b*). Hence, in figure 10, we show additional cases where $Re = 60$, $We = 4$, and λ is held fixed at 100, while ζ takes on three values, $\zeta = 10$, 100 and 1000. The corresponding interior Reynolds numbers are 6, 60, and 600. The most important conclusion, based upon comparing the three parts of figure 10, is that the drop shape and wake structure are hardly changed at all, except for a slight decrease in deformation, and thus a decrease in the size of the recirculating wake. It is not surprising that the drop should become less deformed as ζ increases. With an internal fluid which has a significant density, the interior stagnation pressures will tend to compensate for the exterior stagnation pressure. The only surprise is that the effect of variation of ζ is so weak.

Although the results of figures 5–10 represent variations in all of the four independent dimensionless parameters, we have not yet systematically studied conditions when the internal Reynolds number exceeds the external Reynolds number, that is $\hat{R}e > Re$. This situation is considered in this and the next paragraph, beginning with figure 11, which presents results for $We = 1$, and a very small fixed value of $\lambda = 0.01$, with Re and ζ varied so as to produce internal Reynolds numbers

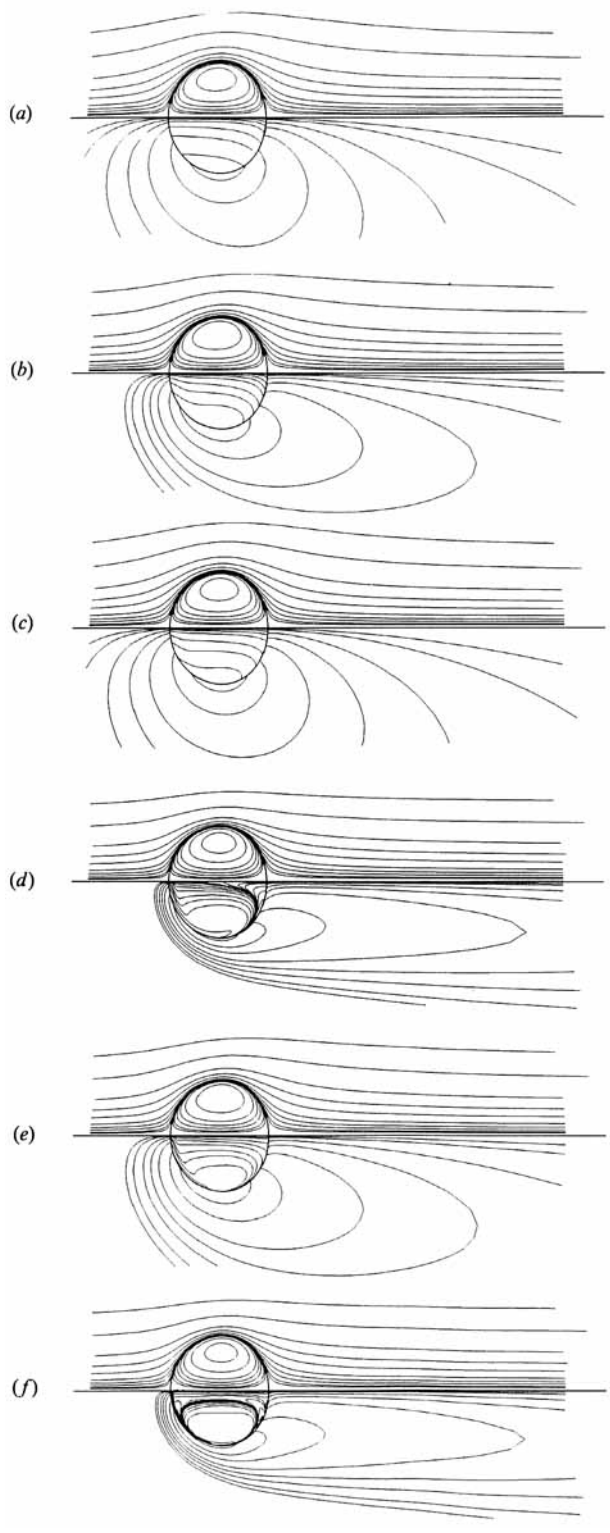

FIGURE 11. Stream function $|\psi| \geqslant 10^{-3}$ and vorticity $|\omega| \geqslant 10^{-2}$ plots for $We = 1$ and $\lambda = 0.01$: (*a*) $Re = 2$, $\zeta = 0.1$, $\hat{Re} = 20$; (*b*) $Re = 10$, $\zeta = 0.1$, $\hat{Re} = 100$; (*c*) $Re = 2$, $\zeta = 0.9$, $\hat{Re} = 182$; (*d*) $Re = 60$, $\zeta = 0.1$, $\hat{Re} = 600$; (*e*) $Re = 10$, $\zeta = 0.9$, $\hat{Re} = 909$; (*f*) $Re = 60$, $\zeta = 0.9$, $\hat{Re} = 5455$.

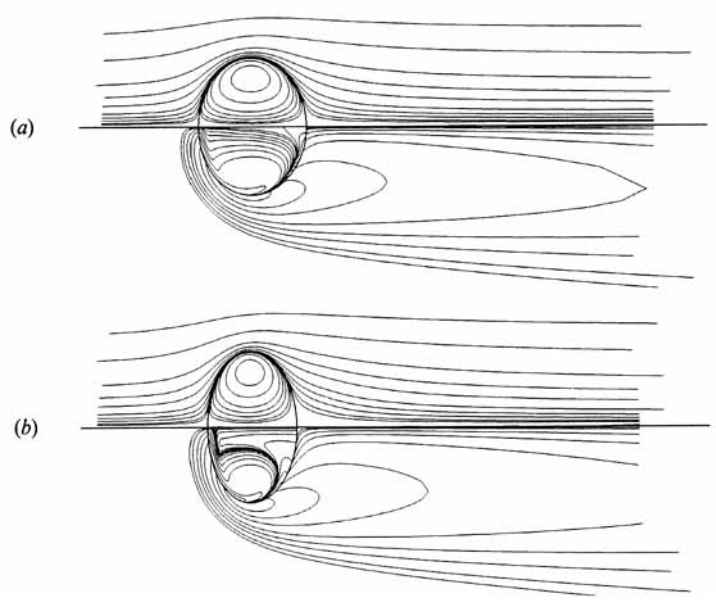

FIGURE 12. Stream function $|\psi| \geqslant 10^{-3}$ and vorticity $|\omega| \geqslant 10^{-2}$ plots for $Re = 60$, $\lambda = 0.01$ and $\zeta = 0.1$ ($\hat{Re} = 600$): (*a*) $We = 2$; (*b*) $We = 4$.

ranging from 18 to 5455. At this Weber number, there is relatively little deformation for any of the cases shown in figure 11. Indeed, the primary change in the solutions is that the inner vorticity lines become increasingly distorted and crowded near the interface – revealing the development of a vorticity boundary layer inside the drop for the larger values of $\hat{Re}$. This is especially evident in the case $Re = 60$, $\lambda = 0.01$, $\zeta = 0.9$ which corresponds to $\hat{Re} = 5455$. In this case, the vorticity gradients are confined to a thin region near the interface, surrounding a constant-vorticity core.

The effect of We for $\hat{Re} > Re$ is illustrated in figure 12. As before, the degree of deformation increases as We increases, but the effect on the flow field is primarily on the internal flow. In both cases, as well as the case $Re = 60$, $We = 1$, $\lambda = 0.01$ and $\zeta = 0.1$ from figure 11, the vorticity inside the drop change sign at the point of maximum curvature, while the exterior vorticity remains negative over the whole of the drop surface. In this regard, the small-λ solutions considered here are fundamentally different from the solutions for $\lambda = 4$, considered previously. In the latter case, it can be seen from the tangential stress condition ($7f$) that $\hat{\omega}_s$ can only change sign if ω_s changes sign. However, for $\lambda = 0.01$ the tangential stress condition does not impose any such constraint.

3.2. *Comparison with experiment*

There have been a relatively large number of experimental studies of the motion of viscous drops in the approximate range of parameters considered in the present work. An attempt to collate the results for drop shape was made by Clift *et al.* (1978) who presented a generalized graphical correlation for drop and bubble shapes. Among the studies that have produced photographs or systematic descriptions of drop shapes as well as some general features of the flow, are Welleck, Agrawall & Skelland (1966), Hendrix, Dave & Johnson (1967), and Satapathy & Smith (1960). Unfortunately, however, direct comparisons with the present solutions cannot be made. Neither Welleck *et al.* nor Hendrix *et al.* provide interfacial tension data, so

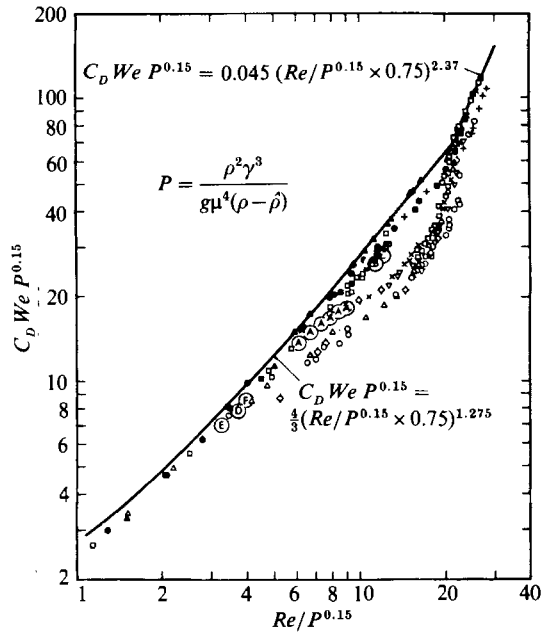

FIGURE 13. Comparison of selected numerical results with experimental observations of Thorsen *et al.* (1968): (A) $We = 1$, $\lambda = 2.5$, $\zeta = 0.91$, $Re = 100, 150, 200, 250, 300, 350$; (B) $Re = 100$, $We = 1$, $\lambda = 2$, $\zeta = 0.5$; (C) $Re = 100$, $We = 0.5$, $\lambda = 1$, $\zeta = 0.02$; (D) $Re = 60$, $We = 0.5$, $\lambda = 4$, $\zeta = 0.91$; (E) $Re = 60$, $We = 1$, $\lambda = 0.01$, $\zeta = 0.001$; (F) $Re = 80$, $We = 0.5$, $\lambda = 4$, $\zeta = 0.91$.

that the Weber numbers are not known. Similarly, Satapathy & Smith fail to list the disperse-phase fluids, and attempt to categorize the drop shape and flow regimes solely as a function of Reynolds number. The most that we can say is that the gross features of the present solutions – that is, flow field and shape – compare favourably with the steady results found in the experimental papers. At low Weber numbers, the shapes of the drops are spheroidal (nearly spherical and elliptical) and at higher values of We the shape tends to a spherical or ellipsoidal cap. At intermediate values of Re, the shape is ellipsoidal in nature, and an appreciably sized recirculating wake forms at the rear of the drop. We have already mentioned the experimental investigations that show a detached wake. In addition to drop shape and general flow features, the other information of greatest practical significance is the drag or terminal velocity.

Thorsen, Stordalen & Terjesen (1968) performed an extensive series of experiments to obtain the terminal velocities of carefully purified organic/water systems. Their aim was to obtain results for both the steady and oscillating regimes. We have reproduced the experimental data of Thorsen *et al.* (their figure 13), and superimposed results from our numerical solutions. The result is shown in figure 13. The solid symbols represent experimental results obtained by Thorsen *et al.* using a surface-active agent, while the light symbols are for pure fluids. Two general conclusions can be made from examination of this figure: first, the numerical results of the present work for small Weber numbers are qualitatively and quantitatively comparable with experimental results. Second, the fact that only the results for low We can be correlated with the experimental results of Thorsen *et al.* indicates that a universal correlation for arbitrary We may not exist.

3.3. *Comparison with other theoretical results*

So far as we are aware, there have been no previous investigations that report theoretical results for the motion of a viscous drop with an arbitrary degree of deformation. Indeed, the only existing analytic solutions are asymptotic results for slightly deformed drops at high and low Reynolds numbers.

An analysis of drops translating through a fluid at large Reynolds number was carried out by Harper & Moore (1968), following an earlier boundary-layer analysis for bubbles due to Moore (1963, 1965). Harper & Moore (1968) showed that the limiting solution for a spherical drop in the limit $Re \to \infty$ is the potential-flow solution outside and Hill's spherical vortex inside, except for thin boundary layers existing near the drop interface, along the axis of symmetry inside the drop, and downstream of the drop in a thin wake extending to infinity. In contrast to this asymptotic flow structure, the present numerical results for finite Reynolds numbers show extensive regions of significant vorticity, with a recirculating wake for sufficiently large We and $Re \gtrsim 60$ that is detached from the drop surface.

Apart from the fact that the wake is detached, the situation is very similar to that described earlier by Ryskin & Leal (1984*a*, *b*) for a deformable bubble/void. In that case, recirculating wakes were also found for finite Reynolds numbers, though boundary-layer analysis indicates that separation should not occur for $Re \to \infty$. Dandy & Leal (1986) later demonstrated that the recirculating wake was strictly a finite-Reynolds-number phenomenon, due to vorticity accumulation behind the bubble, which disappeared for sufficiently large Re. As we have noted earlier, the idea that the recirculating wake does not represent separation in the usual boundary-layer sense is seemingly corroborated by the present solutions, which show recirculation without a point of detachment (separation) on the drop surface. One important difference between the bubble and drop is that vorticity is generated for the drop by both surface curvature (as for the bubble) and no slip in relative proportions that depend on λ. Evidently, one consequence is that sufficient vorticity is generated to produce a recirculating wake for $\lambda \geqslant O(1)$ with relatively little deformation, in sharp contrast to the bubble/void where a threshold level of deformation is required to produce a recirculating wake. The relationship between λ, surface vorticity, and wake structure is particularly striking for the series of solutions in figure 7.

An interesting question, in view of the solutions that we have obtained for relatively large but finite Reynolds numbers, is whether the asymptotic structure found by Harper & Moore (1968) will actually exist for $Re \gg 1$. Specifically, although it is unlikely that a sufficiently small Weber number can be achieved for $Re \gg 1$ to keep the drop from deforming, we might anticipate from Harper & Moore's solution that regions of significant vorticity would be confined to thin boundary layers and wakes for sufficiently large Reynolds number, with no recirculating zone downstream. If true, this would be very much like the behaviour found by Dandy & Leal (1986) for a bubble/void.

To investigate the effect of the Reynolds number on the flow fields at large Re, a series of calculations were done for $We = 1$, $\zeta = 0.91$, $\lambda = 2.5$ and $150 \leqslant Re \leqslant 350$. The idea was to choose a value of We and λ such that the rate of vorticity production might be small enough that convective transport could sweep the vorticity away (and thus 'dissipate' the recirculating wake) at finite Re so that a transition toward the asymptotic structure might be evident numerically. In using second-order centred finite differences there is an upper bound on Re for which (reliable) solutions

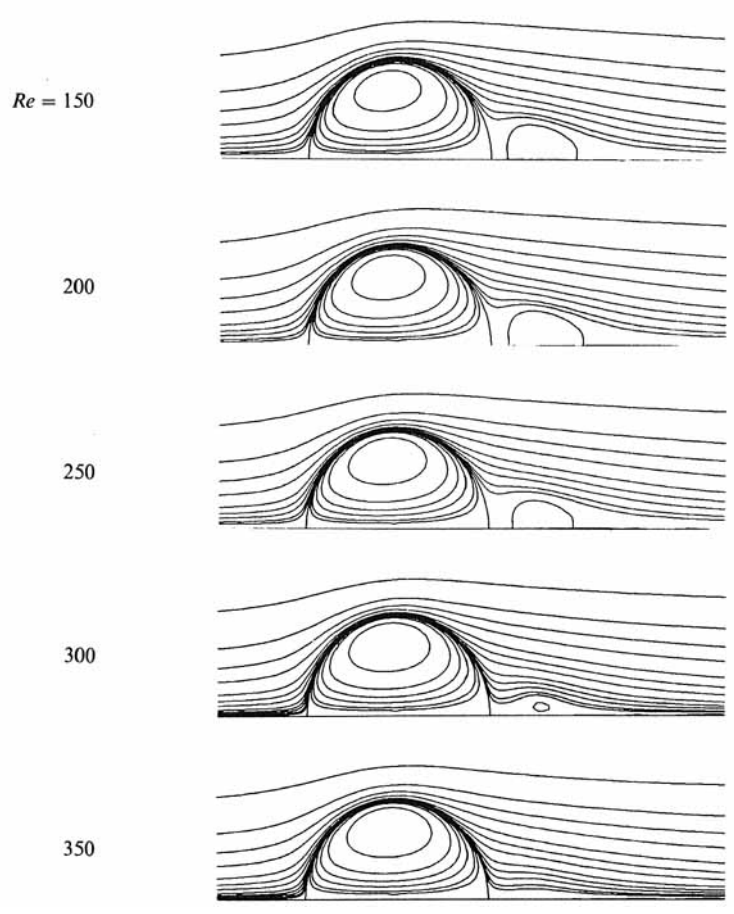

FIGURE 14. The flow field as a function of Re for $We = 1$, $\zeta = 0.909$, and $\lambda = 2.5$.

may be obtained, which in turn depends on the cell Reynolds number (or, a Reynolds number based on the discretization). Thus, a fine mesh will increase the Reynolds number at which a reliable solution can be found. With the discretization used (61×61 mesh, inside and out), and the nearly spherical shapes arising from $We = 1$, we had little trouble finding apparently reliable solutions up to $Re = 400$. Figure 14 shows the flow behaviour as Re is increased: the recirculating wake first appears at a Reynolds number of approximately 60, grows to a maximum length at roughly $Re = 180$, and then completely disappears by the time the Reynolds number reaches 350. Note that as the eddy shrinks in size the vortex inside the drop becomes more fore–aft symmetric, that is, closer to Hill's vortex. We conclude from these solutions that the asymptotic structure found by Harper & Moore will exist for sufficiently large Reynolds number. Comparison of C_D between our numerical solutions and the analytical work of Harper & Moore can be found in table 2 for a variety of Reynolds numbers.

Another interesting aspect of the solutions shown in figure 14 is that for $Re \gtrsim 100$ the drop shape is relatively insensitive to Reynolds number. A similar insensitivity to Re was also observed by Ryskin & Leal in their work on deformable bubbles/voids. Had the shape not been so insensitive to Re, that is, had deformation increased with increasing Reynolds number as was true for lower Reynolds numbers, then it probably would not have been possible to determine anything about the

	C_D	
Re	Harper & Moore	Present work
100	−0.4854	0.912
150	0.3142	0.726
200	0.5192	0.633
250	0.5692	0.570
300	0.5686	0.565
350	0.5502	0.554
400	0.5256	—

TABLE 2. Comparison between analytical results of Harper & Moore (1968) and present work, for $\lambda = 2.5$ and $\zeta = 0.91$. The formula for C_D in Harper & Moore is

$$C_D = \frac{48}{Re}\left\{1+\frac{3}{2V}+\frac{\log Re\,\lambda_b^2(1+V')}{Re^{\frac{1}{2}}}\frac{}{V^2}C_1+\frac{\lambda_b(1+V')}{Re^{\frac{1}{2}}V}\left[\frac{\lambda_b(1+V')}{V}C_2+\left(1+\frac{3}{2V}\right)C_3\right]\right\},$$

where $V = \mu/\hat{\mu} = 0.4$, $V' = (\zeta\lambda)^{-\frac{1}{2}} = 0.66332$, $\lambda_b = (2V+3)/(2V'+3) = 0.878278$, $C_1 \approx 0.120775$, $C_2 \approx 7.099424$, $C_3 \approx -8.745213$.

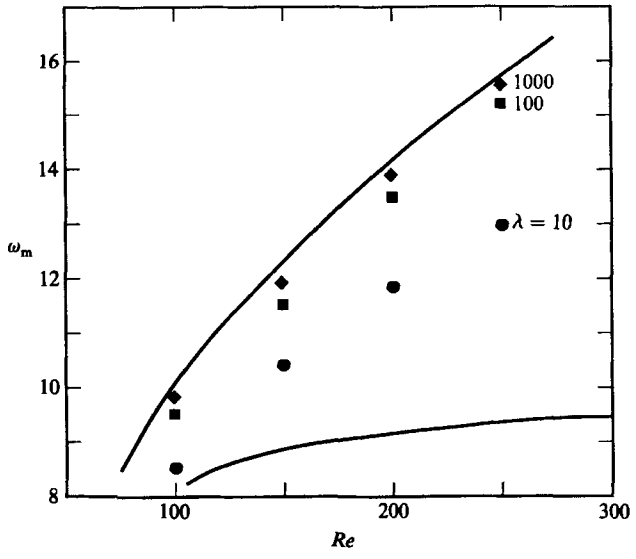

FIGURE 15. Plot of maximum surface vorticity ω_m versus *Re* for several values of the viscosity ratio. The upper solid line is $\omega = Re^{\frac{1}{2}}$ and the lower line is calculated values of ω_m for a void of fixed shape.

correspondence between the results of this work and those of Harper & Moore. A great deal of care was taken to ensure that the numerical results are accurate, and that they do not depend on either numerical parameters or the method used. A much more detailed discussion of the accuracy of the numerical scheme is given in an earlier paper (Dandy & Leal 1986). Of course, the results for other values of *We*, λ and ζ will be different in detail from those exhibited here, but we expect that the same qualitative behaviour would be manifested at sufficiently large *Re* in all cases.

Another point of interest is the Reynolds-number dependence of wake structure and its dependence on λ, i.e. on the relative mix of vorticity production by the boundary curvature and no slip. Theory predicts that in the limit $\lambda \to \infty$, the

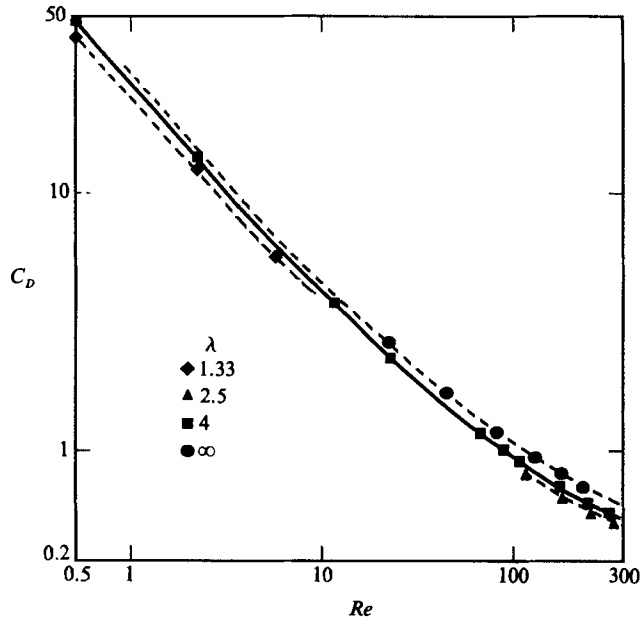

FIGURE 16. Comparison of C_D between numerical results of present work (symbols) and correlation of Rivkind & Ryskin (1976) (curves).

maximum surface vorticity becomes proportional to the square-root of the Reynolds number for $Re \gg 1$, that is, $\omega_m \propto Re^{\frac{1}{2}}$, and in this case, a separated flow with recirculating wake exists even in the limit $Re \to \infty$, as predicted by boundary-layer theory. On the other hand, for $\lambda = 0$, $\omega_m \to$ constant as $Re \to \infty$ for a body of fixed shape, and we showed in an earlier paper that the recirculating wake then disappears for sufficiently large Re, also in agreement with boundary-layer analysis. The solutions for a viscous drop, considered here, provide a basis for examining the transition process where vorticity is produced by some combination of no slip and boundary curvature. In figure 15 we display numerical results from the present work for ω_m at fixed $We = 0.5$, $\zeta = 0.91$ and several different Reynolds numbers: 100, 150, 200 and 250. The upper solid line is $\omega \equiv Re^{\frac{1}{2}}$ and it is apparent that as λ increases, ω_m tends toward an $Re^{\frac{1}{2}}$ dependence. The lower solid line is a plot of numerically calculated values of ω_m as a function of Re, for a void of fixed shape, taken from Dandy & Leal (1986). It is apparent for the void that ω_m asymptotes to a constant as $Re \to \infty$. The fact that convection of vorticity downstream becomes increasingly efficient for increasing Re, while the rate of vorticity production asymptotes to a constant value in this case, may explain the disappearance of the recirculating wake for increasing Re (as shown by Dandy & Leal 1986). Similarly, for $\lambda = O(1)$ the manitude of vorticity ω_m increases much more slowly with Re than for a solid, and this may account for the disappearance of the recirculating wake with increase of Re in these cases.

As a check on our numerical results at higher values of Re, we compare drag coefficients calculated in this work against those of Rivkind & Ryskin (1976) who present a correlation for calculating the drag on a viscous spherical drop, as a function of Re and λ:

$$C_D = \frac{1}{\lambda+1}\left[\lambda\left(\frac{24}{Re}+\frac{4}{Re^{\frac{1}{3}}}\right)+\frac{14.9}{Re^{0.78}}\right]. \tag{8}$$

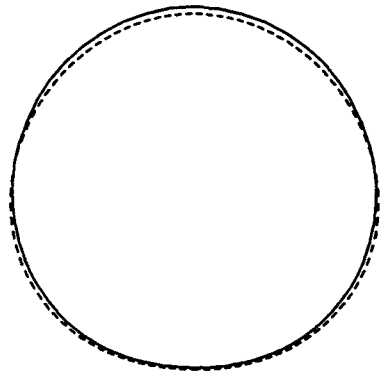

FIGURE 17. Comparison between numerical results of this work at $C_D = 48.4$ (——) and asymptotic analysis of Taylor & Acrivos at $C_D = 48.7$ (– – –) for $Re = 0.5$, $We = 0.5$, $\zeta = 0.909$, and $\lambda = 4$.

We have computed solutions for $We = 0.5$ and $\zeta = 0.91$ and a range of Reynolds numbers $0.5 \leqslant Re \leqslant 300$ at three values of the viscosity ratio: 1.33, 2.5 and 4; some of these solutions are shown in figure 14, the rest are in Dandy (1987). We chose $We = 0.5$ so that the drops would be nearly spherical. We also computed solutions for a solid spherical particle. The results of all of these numerical calculations are compared with the correlation of Rivkind & Ryskin in figure 16. The symbols correspond to our numerical results and the lines to the correlation.

At lower Reynolds numbers (< 1), numerical results are a great deal easier to obtain, and the shapes and flow fields are simpler than at the higher Reynolds numbers. A comparison of a result for $Re = 0.5$, $We = 0.5$, $\zeta = 0.91$ and $\lambda = 4$ with the theoretical prediction of Taylor & Acrivos (1964) is shown in figure 17, where the solid line indicates the result from this work and the dashed line is the result of Taylor & Acrivos. The agreement between the two shapes is pretty good, especially considering that the work by Taylor & Acrivos is an asymptotic analysis which applies only in the limit $Re, We \ll 1$. The drag coefficients compare favourably, with Taylor & Acrivos predicting $C_D = 48.4$, and the numerical results from this work yielding $C_D = 48.7$.

4. Conclusion

The problem solved here demonstrates the viability of a finite-difference technique in conjunction with the grid generation technique of Ryskin & Leal (1983) for the solution of two-fluid free-boundary problems. In the past 15 years a tremendous amount of work has been put into different methods of generating both orthogonal and non-orthogonal coordinate grids (for a review of this work, see Eiseman 1985; Thompson *et al.* 1985), so that there is now a very versatile collection of grid generation techniques available, and no fundamental difficulty in applying finite-difference techniques to complicated (and unknown) domains. As far as we know, however, very little prior work has been done using either finite-difference or finite-element techniques on a two-fluid free-boundary problem at finite Reynolds number. In effect, our numerical technique enables us to perform experiments that would be difficult to carry out in the laboratory: for example, we have the ability to independently vary the four dimensionless parameters that are present in this problem, and the structure of the recirculating wake can be displayed in great detail.

Although the detached recirculating wake structure is not new in the fluid mechanisms literature, it is nevertheless quite novel and its appearance is impossible to understand on the basis of concepts of separation from boundary-layer theory. Indeed, as we have demonstrated, the existence of closed-streamline wakes behind bubbles and drops is strictly a finite-Reynolds-number phenomenon. Another unusual, and as yet unexplained, feature of the solutions for a drop is the lack of correlation between the appearance of a change in sign for the vorticity at the drop surface and the presence of a separation point. This is a unique property of flow past a drop, which is not shared by either solid bodies or bubbles/voids. Other features of the solutions appear to be in accord with qualitative expectations and/or experimental observations. In particular, for a fixed Reynolds number and Weber number, the drop shape became slightly more distorted with decreasing density ratio or viscosity ratio. Further, if a recirculating wake was present, it grew in size when λ was increased, and moved closer to the rear of the drop owing to the slowing of the interior flow. The range of shapes that were observed in this work for $0.5 \lesssim Re \lesssim 300$ and $0.5 \lesssim We \lesssim 15$ were in qualitative agreement with the predictions of the graphical correlation in Clift *et al.* and with direct experimental observation.

All computations were carried out on the CRAY X-MP/24 located at the San Diego Supercomputing Center, and the authors wish to acknowledge the expert help and courtesy shown by SDSC staff member Dr Robert Leary. This work was supported by grants from the Fluid Mechanics Program and the Office of Advanced Scientific Computing at the National Science Foundation.

REFERENCES

Brignell, A. S. 1973 The deformation of a liquid drop at small Reynolds number. *Q. J. Mech. Appl. Maths* **26**, 99–107.

Clift, R., Grace, J. R. & Weber, M. E. 1978 *Bubbles, Drops, and Particles.* Academic.

Christov, C. I. & Volkov, P. K. 1985 Numerical investigation of the steady viscous flow past a stationary deformable bubble. *J. Fluid Mech.* **158**, 341–364.

Dandy, D. S. 1987 Ph.D. Thesis, California Institute of Technology, Pasadena.

Dandy, D. S. & Leal, L. G. 1986 Boundary-layer separation from a smooth slip surface. *Phys. Fluids* **29**, 1360–1366.

Dandy, D. S. & Leal, L. G. 1989 A Newton's method scheme for solving free-surface flow problems. *Intl J. Numer. Meth. Fluids.* (In Press.)

Dorodnitsyn, A. A. & Meller, N. A. 1968 Approaches to the solution of the stationary Navier–Stokes equations. *USSR Comput. Maths Math. Phys.* **8**, 205–217.

Eiseman, P. R. 1985 Grid generation for fluid mechanics computations. *Ann. Rev. Fluid Mech.* **17**, 487–522.

Fornberg, B. 1980 A numerical study of steady viscous flow past a circular cylinder. *J. Fluid Mech.* **98**, 819–855.

Garner, F. H. & Tayeban, M. 1960 The importance of the wake in mass transfer from both continuous and dispersed phase systems. *Anales. Real. Soc., Espan. Fis. Quim.* **B56**, no. 5.

Grosch, C. E. & Orszag, S. A. 1977 Numerical solution of problems in unbounded regions: coordinate transforms. *J. Comput. Phys.* **25**, 273–295.

Harper, J. F. 1972 The motion of bubbles and drops through liquids. *Adv. Appl. Mech.* **12**, 59–129.

Harper, J. F. & Moore, D. W. 1968 The motion of a spherical liquid drop at high Reynolds number. *J. Fluid Mech.* **32**, 367–391.

Hendrix, C. D., Dave, S. B. & Johnson, H. F. 1967 Translation of continuous phase in the wakes of single rising drops. *AIChE. J.* **13**, 1072–1077.

HU, S. & KINTNER, R. C. 1955 The fall of single liquid drops through water. *AIChE J.* **1**, 42–48.

ISRAELI, M. 1970 A fast implicit numerical method for time-dependent viscous flows. *Stud. Appl. Maths* **49**, 327–349.

KANG, I. S. & CHANG, H. N. 1982 The effect of turbulence promoters on mass transfer – numerical analysis and flow visualization. *Intl J. Heat Mass Transfer* **25**, 1167–1181.

LEAL, L. G. 1989 Vorticity transport and wake structure for bluff bodies at finite Reynolds number. *Phys. Fluids* A **1**, 124–131.

LEAL, L. G. & ACRIVOS, A. 1969 The effect of base bleed on the steady separated flow past bluff objects. *J. Fluid Mech.* **38**, 735–752.

LECLAIR, B. P. 1970 Ph.D. thesis, McMaster University, Hamilton, Ontario.

LECLAIR, B. P., HAMIELEC, A. E., PRUPPACHER, H. R. & HALL, W. D. 1972 A theoretical and experimental study of the internal circulation in water drops falling at terminal velocity in air. *J. Atmos. Sci.* **29**, 728–740.

LIGHTHILL, J. 1986 *An Informal Introduction to Theoretical Fluid Mechanics.* Clarendon.

MASLIYAH, J. H. 1970 Ph.D. thesis, University of British Columbia, Vancouver.

MIKSIS, M., VANDEN-BROECK, J.-M. & KELLER, J. B. 1981 Axisymmetric bubble or drop in a uniform flow. *J. Fluid Mech.* **108**, 89–100.

MOORE, D. W. 1959 The rise of a gas bubble in a viscous liquid. *J. Fluid Mech.* **6**, 113–130.

MOORE, D. W. 1963 The boundary layer on a spherical gas bubble. *J. Fluid Mech.* **16**, 161–176.

MOORE, D. W. 1965 The velocity of rise of distorted gas bubbles in a liquid of small viscosity. *J. Fluid Mech.* **23**, 749–766.

MOORE, P. M. & FESHBACH, H. 1953 *Methods of Theoretical Physics.* McGraw-Hill.

NAKAMURA, I. 1976 Steady wake behind a sphere. *Phys. Fluids* **19**, 5–8.

NISI, H. & PORTER, A. W. 1923 On eddies in air. *Phil. Mag.* **46**, 754–768.

OLIVER, D. L. R. & CHUNG, J. N. 1987 Flow about a fluid sphere at low to moderate Reynolds numbers. *J. Fluid Mech.* **177**, 1–18.

PARLANGE, J.-Y. 1970 Motion of spherical drops at large Reynolds numbers. *Acta Mech.* **9**, 323–328.

PEACEMANN, D. W. & RACHFORD, H. H. 1955 The numerical solution of parabolic and elliptic differential equations. *J. Soc. Indust. Appl. Maths* **3**, 28.

PROUDMAN, I. & PEARSON, J. R. 1957 Expansions at small Reynolds numbers for the flow past a sphere and a circular cylinder. *J. Fluid Mech.* **2**, 237–262.

PRUPPACHER, H. R. & BEARD, K. V. 1970 Wind tunnel investigation of the internal circulation and shape of water drops falling at terminal velocity in air. *Q. J. R. Met. Soc.* **96**, 247–256.

RIMON, Y. & CHENG, S. I. 1969 Numerical solution of a uniform flow over a sphere at intermediate Reynolds numbers. *Phys. Fluids* **12**, 949–959.

RIVKIND, V. Y. & RYSKIN, G. 1976 Flow structure in motion of a spherical drop in a fluid medium at intermediate Reynolds numbers. *Fluid Dyn.* **11**, 5–12.

RYSKIN, G. 1980 The extensional viscosity of a dilute suspension of spherical particles at intermediate microscale Reynolds numbers. *J. Fluid Mech.* **99**, 513–529.

RYSKIN, G. & LEAL, L. G. 1983 Orthogonal mapping. *J. Comput. Phys.* **50**, 71–100.

RYSKIN, G. & LEAL, L. G. 1984*a* Large deformations of a bubble in axisymmetric steady flows. Part 1. Numerical techniques. *J. Fluid Mech.* **148**, 1–17.

RYSKIN, G. & LEAL, L. G. 1984*b* Large deformations of a bubble in axisymmetric steady flows. Part 2. The rising bubble. *J. Fluid Mech.* **148**, 19–35.

SATAPATHY, R. & SMITH, W. 1960 The motion of single immiscible drops through a liquid. *J. Fluid Mech.* **10**, 561–570.

SHOEMAKER, P. D. & MARC DE CHAZAL, L. E. 1968 Dimpled and skirted liquid drops moving through viscous liquid media. *Chem. Engng Sci.* **24**, 795–798.

TANEDA, S. 1956 Experimental investigation of the wake behind a sphere at low Reynolds numbers. *J. Phys. Soc. Japan* **11**, 1104–1108.

TAYLOR, T. D. & ACRIVOS, A. 1964 On the deformation and drag of a falling viscous drop at low Reynolds number. *J. Fluid Mech.* **18**, 466–476.

THOMPSON, J. F., WARSI, Z. U. A. & MASTIN, C. W. 1985 *Numerical Grid Generation: Foundations and Applications*. Elsevier.

THORSEN, G., STORDALEN, R. M. & TERJESEN, S. G. 1968 On the terminal velocity of circulating and oscillating liquid drops. *Chem. Engng Sci.* **23**, 413–426.

WELLEK, R. M., AGRAWAL, A. K. & SKELLAND, A. H. P. 1966 Shape of liquid drops moving in liquid media. *AIChE J.* **12**, 854–862.